Understanding the nucleation, assembly and dynamics of axonal actin rings

Maria Leonor Pereira Moura
Aplicações em Biotecnologia e Biologia Sintética
Departamento de Biologia
2023

Supervisor
Mónica Sousa PhD, i3S

Co-supervisor
Ana Rita Costa PhD, i3S


U.PORTO
FACULDADE DE CIÊNCIAS
UNIVERSIDADE DO PORTO

“Enquanto não alcances
Não descanses.”

Miguel Torga

Agradecimentos

Chegando ao fim desta etapa, não poderia de deixar de estar muito agradecida a todos aqueles que contribuíram para a concretização deste trabalho e para o meu imenso crescimento ao longo deste ano.

Gostaria de, em primeiro lugar, agradecer à minha orientadora, Doutora Mónica Sousa. Há pouco mais de um ano atrás entrei no seu gabinete perdida, sem saber muito bem o que queria fazer no meu futuro e talvez até um pouco desencantada com as experiências que me contavam sobre o mundo da ciência. Após cinco minutos de conversa com a Doutora Mónica, senti-me de volta ao meu primeiro ano de faculdade quando o meu sonho era desvendar o que ainda não se sabe, entender como funcionam os alicerces que suportam o mais básico do nosso ser, e ver através do microscópio, aquilo que ninguém viu. Por isso, estou-lhe muito grata por ter despertado em mim a paixão que tinha adormecida, por me ter aberto a porta do seu laboratório, pela disponibilidade constante e todos os ensinamentos que tanto me fizeram crescer e sem quais a conclusão deste trabalho teria sido impossível não teria sido possível.

O meu mais sincero obrigada à Ana Rita Costa, minha coorientadora. Orientar por si só não é uma tarefa fácil, e incluir alguém numa rotina já muito preenchida, é um desafio. No entanto, a Rita não só me orientou como também me acolheu no seu projeto mais querido, dividindo desde cedo tudo comigo, desde a bancada, aos protocolos, até todo o conhecimento que tinha. Sei que não foi fácil, nem sempre as nossas experiências correram bem, nem sempre as células quiseram colaborar connosco, o microscópio também teve os seus dias, mas chegamos ao fim. O amor da Rita pelo que faz é inquestionável e inspirador. Agradeço-te Rita por teres acreditado em mim, por toda a compreensão, carinho e todos os ensinamentos que levo comigo não só para dentro do laboratório, mas para a vida.

Agradeço também aos restantes membros do Nerve Regeneration (Sara, Catarina, Sandra) e do Neurolipid Biology (Pedro, Tiago, Bárbara, Luís) por tudo. Desde os ensinamentos, ao apoio, à companhia, à partilha constante de experiências. Não há sentimento melhor do que chegar todos os dias ao laboratório e nunca me sentir sozinha porque sabia que tinha sempre alguém disponível para me ajudar. Sara, foi uma honra cruzar caminho contigo e espero um dia ser tão boa cientista quanto tu és, obrigada não só por tudo o que me ensinaste, mas por teres sido como uma irmã mais velha dentro deste laboratório. Tiago, duvido que alguma vez me cruze com um colega de laboratório com tanto conhecimento quanto tu tens, mas, se alguma vez isso acontecer, tenho a

certeza que não será tão bom professor como tu foste. Obrigada também ao grupo Nerve Degeneration, Márcia e Marina, pela paciência e por me ajudarem sempre que necessitei.

Não podia deixar de agradecer a uma das melhores partes desta aventura, os quatro novos amigos que ganhei e que levo para a vida. Se este laboratório foi a minha casa, então vocês foram a minha família. Um obrigado geral aos quatro por me limparem as lágrimas, ouvirem os meus mil e um problemas, estarem comigo na casa de banho enquanto me maquilhava, resolverem os meus desastres, me obrigarem a comer quando o apetite não era muito, rirem comigo, festejarem as minhas conquistas e me porem sempre o maior sorriso na cara. Obrigada, Eduardo, meu "co-co-co-orientador", roomie de secretária e parceiro de aventuras. Nunca pensei que algum dia ia gostar tanto de partilhar uma secretária e uma extensão elétrica com alguém, mas não podia ter pedido alguém melhor para partilhar o meu espaço e os meus dias. Obrigada, Vítor, por seres o meu soul twin aqui dentro, por me entenderes antes mesmo de eu falar, fazeres comigo o melhor treino de pernas e me deixares invadir o teu espaço pessoal com os meus abraços diários. Obrigada, Ritinha, por vires equilibrar o poder feminino, mas acima de tudo por me mostrares o que é girl power e o que é ser puramente boa e me inspirares todos os dias a ser melhor. Obrigada, Zé, porque sei que estavas sempre atento e pronto para ajudar mal eu mostrasse o mínimo sinal de necessidade e com a mesma rapidez me fazias dar uma gargalhada que levava tudo de mau que estivesse a sentir. Estou-vos eternamente grata.

O meu próximo agradecimento vai para as minhas amigas do coração que me fizeram sempre acreditar que era mesmo o meu destino entrar em Biologia no ano de 2017. Carolina, Marta, Debs, Sofs, Ferraz e Gi, não há palavras para descrever não só o vosso apoio este ano, mas ao longo destes 5 anos de amizade. Nunca importará se uma está na África, outra a explorar a Argentina, ou do outro lado do mundo, vocês serão sempre as minhas amigas. Um especial agradecimento à Carolina que é desde há alguns anos a minha twin em todos os níveis, a minha confidente e a que mais me atura.

João, acho que para ti não chega agradecer. Nada disto teria sido possível sem o teu constante apoio, sem as tuas palavras motivadoras todos os dias, sem nunca me prenderes, mas ao invés me dares o empurrão que faltava para eu voar. Obrigada por me teres ouvido sempre, mesmo quando não concordavas comigo e me teres dado a força que precisava para continuar. Estou muito agradecida por toda a força que me deste ao longo deste processo, sempre com muito amor, amizade e carinho.

Agradeço a todos os meus professores, que contribuíram para a minha formação e me equiparam com as ferramentas necessárias para conseguir chegar aqui. Um especial agradecimento à Professora Paula Tamagnini que com muita paciência me ajudou a encontrar o caminho em que agora estou e sem a qual não o teria conhecido.

O meu último agradecimento vai para a minha família. Não seria nada sem vocês, e todos à sua maneira, contribuíram para a Leonor que sou hoje e para que chegasse até este ponto da minha vida. Avó, obrigada por me mostrares o que é ser uma mulher, o que é educar, e por seres para sempre o meu modelo a seguir. Madrinha, quando digo que sou filha única penso sempre para mim que na verdade não sou, porque sempre foste como uma irmã mais velha que desde sempre admirei e que desejava ser quando fosse grande, obrigada por todo o apoio, por me deixares ir para tua casa e libertar-me do dia de trabalho e confiares sempre em mim mesmo quando eu não o fazia. Pais, para vocês eu não quero só agradecer, eu quero dar-vos tudo do mundo porque devo-vos tudo o que eu sou. Não há maior prova de amor do que me darem tudo o que podem para que eu tenha a melhor vida possível e me proporcionarem as melhores oportunidades. Obrigada porque acreditaram em mim, por me incentivarem, por me educarem por me acalmarem e reconfortarem no vosso colo que cura tudo. Viram-me batalhar muito ao longo deste ano e foram quem mais viveu esta aventura comigo. Esta tese não é só minha, mas também vossa.

Part of this work was presented at:

Encontro de Investigação Jovem (IJUP), University of Porto,

May 11th 2023

Resumo

Com o avanço da microscopia de super-resolução, um arranjo único do citoesqueleto de actina, o esqueleto periódico membranar (MPS), foi identificado nos neurónios. O MPS é uma rede complexa de anéis de actina interligados por tetrâmeros de espectrina, fornecendo suporte mecânico aos axónios. Dados de trabalhos anteriores indicam que o MPS é uma rede de actina e miosina, capaz de controlar a expansão e contração axonal, sendo crucial na regulação do diâmetro axonal. Atualmente, a nucleação e o arranjo da actina dentro dos anéis ainda não são totalmente compreendidos. Este trabalho tem como foco investigar o papel de diferentes nucleadores de actina, Arp2/3 e forminas, responsáveis pela polimerização ramificada e linear da actina, respetivamente, na formação e manutenção dos anéis de actina do MPS. Para isso, neurónios primários do hipocampo em diferentes dias de cultura in vitro (DIVs) foram tratados com fármacos complementares, CK869 e SMIFH2, que inibem Arp2/3 e forminas, respetivamente. Além disso, também avaliamos como Arp2/3 e forminas afetam a nucleação dos anéis de actina usando abordagens genéticas (shRNA e CRISPR-Cas9). A análise utilizando microscopia de super-resolução, nomeadamente tau-STED, indica que a formação de MPS está comprometida pela inibição da Arp2/3 e das forminas. Além disso, a inibição pelo CK869 em DIVs mais tardios também compromete a manutenção do MPS. Os nossos dados sustentam que o MPS é uma rede de filamentos de actina ramificados e lineares. Os resultados descritos neste trabalho sugerem que a ação complementar dos nucleadores de actina é necessária para a construção do MPS, como nos anéis de actina formados em outros contextos biológicos.

Palavras-chave: anéis de actina; super-resolução; axónios.

Abstract

With the advent of the super-resolution microscopy, a unique arrangement of the actin cytoskeleton, the membrane periodic skeleton (MPS), was identified in neurons. The MPS is a complex network of actin rings interlinked by tetramers of spectrin, providing mechanical support to axons. Our previous data indicate that the MPS is an actomyosin network, able to control axonal expansion and contraction, being crucial in the regulation of axonal diameter. Currently, actin nucleation and arrangement within actin rings remain to be fully understood. This work focuses on investigating the role of different actin nucleators, Arp2/3 and formins, responsible for the branched and linear actin polymerization, respectively, in the formation and maintenance of the MPS actin rings. For that, hippocampal primary neurons were treated, on different days in vitro (DIVs), with complementary drugs, CK869 and SMIFH2, which inhibit Arp2/3 and formins, respectively. Moreover, we are also evaluating how Arp2/3 and formins affect actin rings nucleation by using genetic approaches (shRNA and CRISPR-Cas9). Analysis using super-resolution microscopy, namely tau-STED, indicates that the MPS formation is compromised either by inhibiting Arp2/3 or formins. Moreover, Arp2/3 inhibition at later DIVs also compromises MPS maintenance. Our data supports that the MPS is a network of branched and linear actin filaments. Our results suggest that the complementary action of actin nucleators is needed to provide for the timely MPS assembly, as in actin rings formed in other biological contexts.

Keywords: actin rings; super-resolution; axons

Table of Contents

List of Tables

List of Figures

List of Abbreviations

ABP	Actin- Binding Protein
ADP	Adenosine Diphosphate
AIS	Axon Initial Segment
Arp2/3	Actin-Related Protein 2 and 3 Complex
ATP	Adenosine Triphosphate
cDNA	Complementary DNA
C-domain	Central domain
CC	Coiled Coil Region
CNS	Central Nervous System
DAD	Diaphanous Autoinhibitory Domain
DAPI	4',6-Diamidino-2-Phenylindole
DD	Dimerization Domain
DID	Diaphanous Inhibitory Domain
DIV	Day(s) In Vitro
DMEM	Dulbecco's Modified Eagle Medium
E	Embryonic Day(s)
EU	European Union
EGFP	Enhanced GFP
F-actin	Filamentous Actin
FBS	Fetal Bovine Serum
G-actin	Globular Actin
GIs	GABAergic interneurons
GTP	Guanosine Triphosphate
HBSS	Hank's Balanced Salt Solution
IF	Intermediate Filaments
MT	Microtubule
NF	Neurofilament
PBS	Phosphate-Buffered Saline
P/S	Penicillin-Streptomycin
PFA	Paraformaldehyde
PLL	Poly-L-Lysine
PNS	Peripheral Nervous System
Rho	Ros Homolog Family Member A
RT	Room Temperature

SEM	Standard Error of The Mean
shRNA	Small Hairpin RNA
STED	Stimulated Emission Depletion Microscopy
VASP	Vasodilator- Stimulated Phosphoprotein
WASP	Wiskotl-Aldrich Syndrome Protein
WAVE	Wasp- Family Verprolin- Homologous Protein
WHAMM	WASP Homologue-Associated Protein with Actin, Membranes and Microtubules
WT	Wild-Type

Introduction

1. The Nervous System

The Nervous System is the most complex within biological systems (Koch & Laurent, 1999). It transmits signals between the brain and the body's various organs essential to regulate fundamental functions such as movement, breathing, vision, and cognition, thus governing our existence (Bazira, 2021). It includes two main parts: the central nervous system (CNS) and the peripheral nervous system (PNS) (Ludwig & Varacallo, 2018).

The CNS includes the brain, spinal cord and optic nerves as shown in magenta in Figure 1. The PNS comprises the cranial nerves, spinal nerves, the ganglia associated with the cranial and spinal nerves, the right and left sympathetic chains and their ganglia, and the pelvic parasympathetic nerves as illustrated in blue in Figure 1 (Bazira, 2021; Ludwig & Varacallo, 2018).

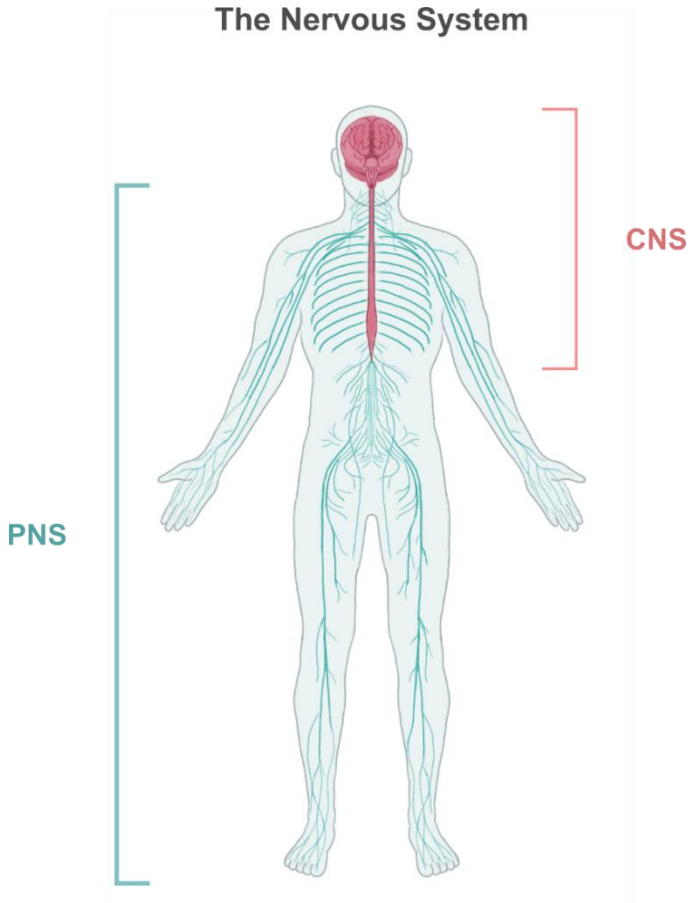

Figure 1 – Schematic representation of the Nervous System. The Central Nervous System (CNS) is shown in red and it includes the brain, spinal cord and optic nerves. The Peripheral Nervous System (PNS) in blue comprises the cranial nerves, spinal nerves, the ganglia associated with the cranial and spinal nerves, the right and left sympathetic chains and their ganglia, and the pelvic parasympathetic nerves.

2. The Neuron – The Building block of the Nervous System

Neurons emerge as the fundamental unit in the Nervous System (Brodal, 2004). These specialized cells are the principal players in transmitting and processing information, enabling the nervous system to carry out its diverse functions seamlessly (Bazira, 2021). Neurons are structurally distinct from most other cells, being able to rearrange and assemble into neuronal circuits and propagate signals due to their unique capability of polarizing (Bradke & Dotti, 2000; Lovinger, 2008; Tahirovic & Bradke, 2009) As illustrated in Figure 2, each neuron consists has four main compartments, the cell body, dendrites, axon and growth cone/synaptic terminals which will be further briefly discussed.

2.1 The main components of the Neuron

2.1.1 The Cell Body (Soma)

The cell body, often designated soma, is the central region of the neuron. It contains the nucleus and the majority of the cellular organelles (Hammond, 2015). The soma is responsible for the essential metabolic functions of the neuron. It is the main site of protein synthesis and energy production that are critical for neuron survival and function (Dharani, 2015; Ludwig & Varacallo, 2018). The cell body also receives and integrates signals from the dendrites. Soma's size and shape vary depending on the type of neuron and its function. For example, motor neurons that control muscle movement have larger cell bodies than sensory neurons that detect environmental stimuli (Hammond, 2015).

2.1.2 Dendrites

Dendrites are branching extensions that extend from the cell body. They are specialized expansions of the neuron receiving input from other neurons or sensory receptors (Duch & Ryglewski, 2016). Dendrites are highly branched, and covered with synapses, which are specialized junctions that allow for communication between neurons. Depending on the type of neuron and on its function, dendrites can vary in size, shape and number (Mihailoff & Haines, 2018; Purves & Lichtman, 1985). Additionally, several factors, including changes in synaptic input (Tavosanis, 2012), activity-dependent signalling pathways (Duch & Ryglewski, 2016; Tavosanis, 2012) and environmental factors (Tavosanis, 2012) have been described to affect dendrite size. For example, neurons tend to only keep branches that have functional connections with other neurons and retract the remaining, as it is a more efficient use of their resources and energy (Tavosanis, 2012). Also, dendritic trees of GABAergic interneurons (GIs) grow in

size to handle an increased number of incoming synaptic inputs (Libersat, 2005). Another example is the regulation of calcium-dependent signalling pathways in neurons, that can lead to the generation of calcium waves. These waves, in turn, are associated with the stabilization of newly formed neuronal branches or filopodia (Tavosanis, 2012). Furthermore, the exposure to environmental enrichment and training can lead to structural changes in dendrite organization in the mammalian brain, including in humans (Tavosanis, 2012).

2.1.3 The Axon

The axon extends from the cell body as a long neuronal process that can travel a few micrometers to over a meter in humans. Axons specialize in transmitting electrical impulses, known as action potentials, to the neighbouring sites of synaptic interaction. The rapid transmission of these electrical signals is assured by a myelin sheath that insulates the axon (Baas & Lin, 2011; Debanne et al., 2011; Neukirchen & Bradke, 2011; Purves, 2004; Squire, 2013).

Myelinated axons are described as having three distinct segments represented in Figure 2: the axon initial segment (AIS), where somatic inputs accumulate and trigger the onset of an action potential, a myelinated shaft, which is responsible for consistently conveying information in the form of sequences of action potentials and a terminal segment, known as the preterminal axon, which encompasses the synaptic terminal (Debanne et al., 2011; Purves, 2004).

The AIS

The AIS is a unique portion of the axon located near the cell body, typically positioned within the initial 20-60 micrometers of the axon. This strategic positioning demarcates the boundary between the somatodendritic and axonal compartments, thereby preserving the unique molecular characteristics inherent to each (Jones & Svitkina, 2016; Leterrier, 2016, 2018). The AIS includes a wide and adaptable complex of proteins, including ankyrin G, a central organizer of this structure (Leterrier, 2016), membrane proteins (Leterrier, 2018), scaffold proteins (Huang & Rasband, 2018), and cytoskeletal adaptors (Leterrier, 2018) that respond dynamically to developmental and physiological cues (Huang & Rasband, 2018; Jones & Svitkina, 2016; Leterrier, 2016, 2018; Yamada & Kuba, 2016). The AIS is involved in the formation of the action potentials and in filtering selective cargo transport from the cell body into the axon (Huang & Rasband, 2018)

Within the AIS, actin assumes a critical role by functioning as a selective transport filter (Leterrier, 2016). Recent experimental evidence underscores this role, demonstrating that dendritic cargoes exhibit comparable frequencies of entry into both dendrites and the axon. However, it is within the AIS that their continued trafficking is contingent upon actin-mediated mechanisms. According to this model, cargoes harboring active myosin motors are effectively sequestered within the AIS through anchorage to actin patches. (Huang & Rasband, 2018; Leterrier, 2018) The presence of these actin patches within the AIS lends empirical support to this conceptual framework. The significance of actin within the AIS is further underscored by research findings indicating that disruptions in the actin filter result in the loss of polarized cargo transport, impacting both axonal and dendritic cargoes. (Huang & Rasband, 2018; Jones & Svitkina, 2016)

The Axon Shaft

Moving distally from the AIS, the remaining portion of the axon is called the axon shaft (Leterrier et al., 2017). It comprises microtubules, neurofilaments, and actin filaments (Leterrier, Dubey, & Roy, 2017). The distinctive unipolar arrangement of microtubules (MTs) within the axon plays a vital role in facilitating the anterograde transport of various cargo, guided by kinesins targeting the plus ends of MTs. Various mechanisms exist to finely regulate the activity of kinesins (Conde & Cáceres, 2009; Leterrier et al., 2017). In addition, the axon houses an actin cytoskeleton beneath the axonal plasma membrane. This actin framework offers the axon both and stable support (Leterrier et al., 2017; Roy, 2016).

Regarding its length, the extent of the axon varies in accordance with the neuron's function. For example, spinal cord neurons typically possess lengthy axons, ranging from several millimeters to meters. Conversely, interneurons, which operate within localized circuits, exhibit shorter axonal extensions, typically spanning only several millimeters (Muzio & Cascella, 2022; Prokop, 2020; Roy, 2016). The shaft's different components allow this structure to play its pivotal role of conducting electrical impulses towards synapses with dendrites or cell bodies of other neurons, as well as non-neuronal targets like muscle fibers (Debanne et al., 2011; Muzio & Cascella, 2022; Yuan et al., 2012).

Axon Terminals

Axons culminate in a specialized structure called the axon terminal, also referred to as the presynaptic terminal. At this terminus, a pivotal transformation occurs, where electrical signals are transmuted into chemical signals. These chemical signals

encompass neurotransmitters, neuromodulators, or neurohormones, serving as messengers that traverse the synapse or neuromuscular junction (Ludwig & Varacallo, 2018).

The axon terminal, which plays a central role in ensuring precise excitation-release coupling, is also subject to activity-dependent regulation. This regulatory mechanism, has the potential to alter the temporal characteristics of neuronal spikes, potentially resulting in spike broadening (Debanne et al., 2011). This dynamic aspect underscores the adaptability of neurons and their ability to fine-tune their signaling processes in response to varying levels of neural activity (Südhof, 2012). The axon terminals, in their role as information transmitters, adeptly modulate neurotransmitter secretion by modifying factors such as the number, localization, and molecular composition of synaptic vesicles (Terni & Llobet, 2021).

The journey of information initiation at a presynaptic terminal occurs through an action potential, ultimately culminating in the transmission of chemical neurotransmitters to the postsynaptic cell (Südhof, 2012). Within the presynaptic terminal, these neurotransmitters are carefully packaged into synaptic vesicles. When an action potential activates presynaptic voltage-gated Ca^{2+} channels, the neurotransmitters are released via Ca^{2+} triggered synaptic vesicle exocytosis into the synaptic cleft. In this synaptic cleft, they activate postsynaptic receptors, thus transmitting the information (Purves, 2004; Squire, 2013; Südhof, 2012).

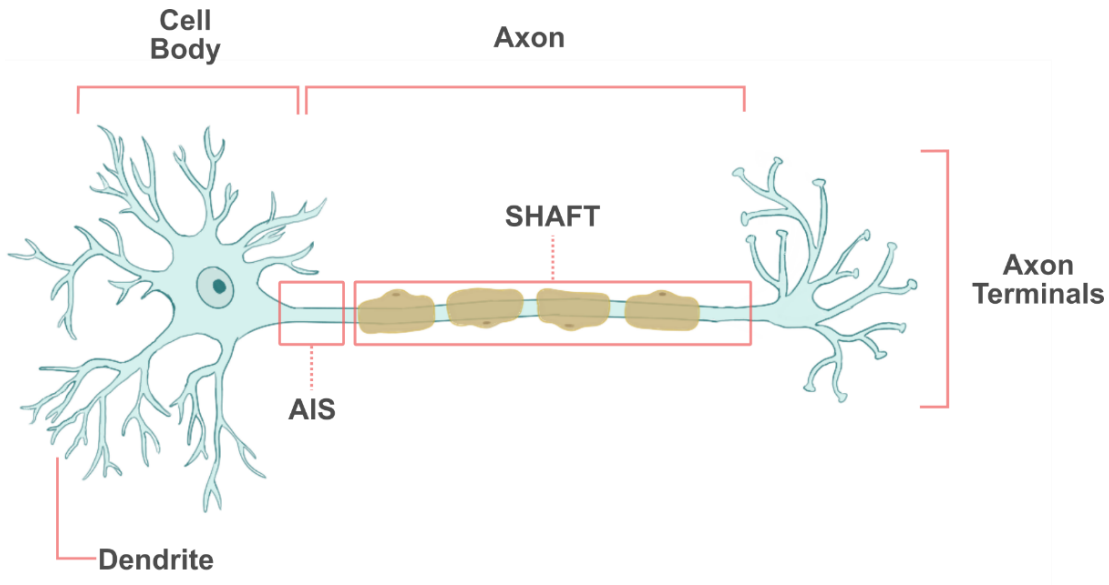

Figure 2 – Schematic representation of the Neuron's main compartments: Cell Body, Axon, Dendrite and Axon Terminals. Organization of the myelinated axon: the axon initial segment (AIS) and a myelinated SHAFT.

2.2 Neuronal polarization

Neurons undergo a profound metamorphosis after their birth and differentiation. This transformation involves rearranging their initial symmetrical form, undergoing dramatic structural changes, and establishing distinct axonal and dendritic territories, each with its own unique attributes and functions (Arimura & Kaibuchi, 2007; Bradke & Dotti, 2000; Tahirovic & Bradke, 2009).

Neuronal polarity refers to the complex process by which a neuron develops a single axon and multiple dendrites, allowing them to communicate with each other and with other cells in the body (Bradke & Dotti, 2000; Tahirovic & Bradke, 2009; Takano et al., 2015; Witte & Bradke, 2008). This process is crucial for the assembly of functional neuronal networks in the developing animal and involves the formation of specialized areas in the plasma membrane and the specific organization of the cytoplasm underlying these areas (Bradke & Dotti, 2000; Tahirovic & Bradke, 2009; Takano et al., 2015). The establishment of neuronal polarity can be studied using dissociated hippocampal neurons derived from embryos *in vitro*. The development into these different stages (Figure 3) involves a variety of intracellular mechanisms and molecular signals. (Bradke & Dotti, 2000)

After plating, stage 1 initiates with neurons assuming a round shape bearing thin lamellipodia, then they develop into stage 2, by which they transform into multipolar cells (Arimura & Kaibuchi, 2007; Tahirovic & Bradke, 2009; Takano et al., 2015). This begins with the establishment of asymmetry in the cell, which is thought to be triggered by extracellular cues such as growth factors and extracellular matrix molecules (Bradke & Dotti, 2000). This asymmetry leads to the formation of a specialized structure called the growth cone at the tip of the extending neurite and, within 24 to 48 hours, stage 3 occurs: one neurite enlarges its growth cone and extends rapidly to become the axon (Arimura & Kaibuchi, 2007; Tahirovic & Bradke, 2009; Takano et al., 2015). The destabilization of the actin cytoskeleton in the growth cone of the developing axon, allows microtubules to polymerize and protrude more distally, eventually leading to the elongation of the axon (Tahirovic & Bradke, 2009). Moving to stage 4: the remaining shorter neurites will develop into dendrites. At stage 5 it is possible to observe the functional maturation and formation of dendritic spines and synapses. Finally, at stage 6 the formation of dendritic spines continues (Arimura & Kaibuchi, 2007; Bradke & Dotti, 2000; Takano et al., 2015).

The destabilization of the actin cytoskeleton is regulated by intracellular signaling pathways, including the Ros Homolog Family Member A (Rho) family of GTPases, which can activate or inhibit actin polymerization and depolymerisation (Bradke & Dotti, 2000; Tahirovic & Bradke, 2009; Witte & Bradke, 2008). For example, the activation of the

RhoA pathway can lead to the formation of actin stress fibers and to the stabilization of the actin cytoskeleton, while the activation of the Cdc42 pathway can lead to the formation of filopodia and the destabilization of the actin cytoskeleton (Arimura & Kaibuchi, 2007; Bradke & Dotti, 2000; Takano et al., 2015; Witte & Bradke, 2008). In addition to regulating actin dynamics, intracellular signalling pathways can also modulate membrane trafficking and fusion events that are critical for the establishment of neuronal polarity (Tahirovic & Bradke, 2009). Rac, a member of the Rho family of GTPases, modulates the activity of a small guanosine triphosphate (GTP) binding protein, Arf6 (ADP-ribosylation factor 6) that has as primary function cellular membrane recycling. When Arf6 is inactive, the binding of GTP is not effective and it impedes the formation of Rac-induced cellular protrusions. This hints at the potential of Rho proteins to coordinate cellular membrane traffic (Bradke & Dotti, 2000)

In summary, the establishment of neuronal polarity is a complex and dynamic process. It intricately relies on the interplay of numerous intracellular signalling pathways and membrane trafficking events. Moreover, it is essential to underscore that without the cytoskeleton, this process would be unattainable (Witte & Bradke, 2008).

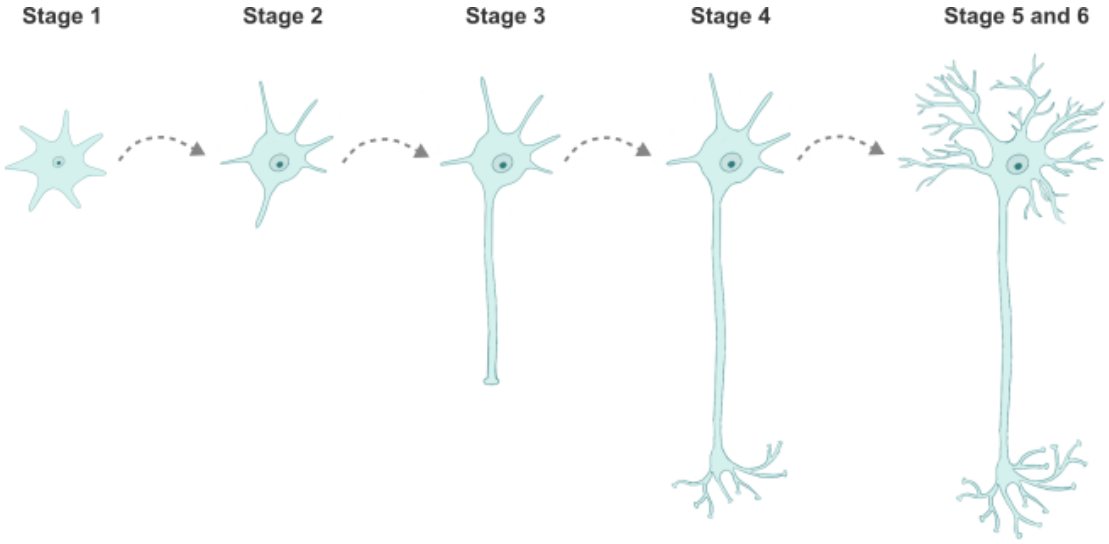

Figure 3- Schematic drawing of the neuronal polarization stages. The stages of polarization illustrated were first described by Banker and its team in 1994 using cultured rat embryonic hippocampal neurons (Craig & Banker, 1994). Immediately after plating, stage 1 initiates and neurons start as round cells with lamellipodia. In the stage 2, they transform into multipolar cells, establishing cellular asymmetry triggered by extracellular cues. Next, at stage 3, one neurite enlarges its growth cone and becomes the axon, with the destabilization of the actin cytoskeleton allowing axon elongation. At stage 4, the remaining shorter neurites develop into dendrites. Finally at stage 5 the functional maturation occurs, and dendritic spines and synapses form. Culminating in stage 6 where the formation of dendritic spines continues.

3. The Cytoskeleton

The cytoskeleton is a complex network of protein filaments that provides structural support and maintains the shape of a cell. Apart from its structural function, the cytoskeleton also plays a crucial role in facilitating various forms of cellular movement. This encompasses not only the mobility of whole cells but also the internal transport of organelles and other cellular components (Conde & Cáceres, 2009; Cooper & Adams, 2023). As illustrated in Figure 4 it comprises three major constituents: microtubules, neurofilaments, and actin filaments (or microfilaments), briefly discussed in the following section. Despite presenting its own set of properties and distinct roles, the different components can interconnect, thus forming a dynamic and adaptative network, fundamental to its associated functions (Leite & Sousa, 2016; Leterrier et al., 2017; Menon & Gupton, 2016; Stiess & Bradke, 2011). The axon cytoskeleton participates in axon formation (Neukirchen & Bradke, 2011), transport, polarization (Stiess & Bradke, 2011) and maintenance of the structural integrity of specific structures such as the AIS and presynaptic boutons (Kevenaar & Hoogenraad, 2015; Leterrier et al., 2017; Menon & Gupton, 2016; Neukirchen & Bradke, 2011; Stiess & Bradke, 2011).

3.1 Microtubules

Microtubules (MTs) are thin, long, polarized and hollow structures composed of 13 protofilaments of α/β-tubulin heterodimers (Leterrier et al., 2017; Menon & Gupton, 2016). These structures participate in numerous cellular processes. For example, they play a crucial role in axonal transport, being the railroads for molecular motors (Conde & Cáceres, 2009), they allow the maintenance of the structural integrity of axons (Leterrier et al., 2017). Additionally, MTs are essential players in cell division, orchestrating the orderly segregation of genetic material (Leterrier et al., 2017). These dynamic structures exhibit polarity, with a fast-growing 'plus' end and a slower-growing 'minus' end, allowing them to adapt to the changing needs of the cell (Kevenaar & Hoogenraad, 2015). Together with actin filaments, MTs play a pivotal role in axon specification and growth (Conde & Cáceres, 2009), forming the dynamic infrastructure of the cytoskeleton and continuously reshaping the cellular landscape (Conde & Cáceres, 2009; Leterrier et al., 2017).

3.2 Neurofilaments

Neurofilaments, as the intermediate filaments within neurons, are essential to maintain the structural integrity of neurons (Menon & Gupton, 2016; Yuan et al., 2009).

These structural components, measuring approximately 10 nm in diameter, are complex heteropolymers consisting of subunits of high, medium, and low molecular weights and internexin or peripherin intermediate filaments (Leterrier et al., 2017; Prokop, 2020). Each neurofilament subunit exhibits a distinctive structure, encompassing a short amino-terminal globular head domain, a central and evolutionarily conserved alpha-helical rod domain, and a variable carboxy-terminal tail domain (Yuan et al., 2012). The central rod domain co-assembles with other subunits to create dimers, protofilaments, and, ultimately, the mature neurofilament (Leterrier et al., 2017). Remarkably, in contrast to actin and microtubules, neurofilaments lack polarity and do not rely on adenosine triphosphate (ATP) or GTP for polymerization (Leterrier et al., 2017). The primary role of neurofilaments is related to the regulation of axon diameter, thus ensuring efficient electrical signal propagation in neurons (Kevenaar & Hoogenraad, 2015; Leterrier et al., 2017).

3.3 Actin and Actin Binding Proteins

Actin is one of the most prevalent proteins in cells. Its primary location is the cytoplasm, though it also extends its presence into the nucleus. Actin is involved in a variety of cellular processes, including alterations in cell shape, motor-based organelle transport, regulation of ion transport, and receptor-mediated responses of the cell to external signals (Dominguez & Holmes, 2011; Lappalainen, 2016; Menon & Gupton, 2016; Merino et al., 2020; Pollard, 2016).

Within cells, actin exists in two main forms: monomeric (G-actin) and filamentous (F-actin), and both can bind ATP or adenosine diphosphate (ADP, respectively). When G-actin binds ATP and reaches a critical concentration, it undergoes a conformational change that allows it to polymerize into F-actin (helical polymer of G-actin subunits that can form long, thin filaments). The actin filaments can grow in both ends, the barbed and minus end. However these are not the same chemically, in fact the amount G-actin needed for the barbed end to grow is lower than the amount of G-actin needed for the minus end to grow. .(Menon & Gupton, 2016) This difference affects how actin molecules come together and explains the actin treadmill process. In this process, actin is continuously polymerized at the barbed ends and depolymerized at the pointed ends during this dynamic process known as "actin treadmilling," which maintains filament length in a stable cellular environment (Menon & Gupton, 2016; Pollard, 2016). In its polymerized form, F-actin exhibits a distinct polarity: the "barbed-end" primarily consists of ATP-bound actin subunits, marking the filament's newer segment, while the "pointed-end" is characterized by the prevalence of ADP-bound subunits, corresponding to the

filament's older segment. All these biological processes are regulated by actin-binding proteins (ABPs). (Pollard, 2016) The ABP family comprises significantly heterogeneous and high-numbered (approximately 162) molecules. Depending on their role, ABPs are categorized into several groups (Dominguez, 2004; Pollard, 2016; Remedios et al., 2003; Uribe & Jay, 2009) sequesters or G-actin subunits binders, thus preventing actin polymerization (Dominguez & Holmes, 2011; Hannappel, 2007; Remedios et al., 2003; Witke et al., 1998); ii) nucleators, such as formins and Arp2/3, catalysing the nucleation and actin elongation; iii) F-actin barbed (Leite et al., 2016a) and pointed end capping proteins preventing the polymerization or triggering depolymerization (Gregorio et al., 1995; Rao et al., 2014; Remedios et al., 2003; Yamashita et al., 2003); iv) F-actin bundlers, cross-linkers and stabilizers, including actinin and filamin (Lappalainen, 2016; Pittenger et al., 1994; Remedios et al., 2003; Sutherland-Smith, 2011); v) actin filament severing proteins, such as gelsolin and ADF/cofilin (Dominguez & Holmes, 2011; Ghoshdastider et al., 2013; Remedios et al., 2003; Sun et al., 1999; Wioland et al., 2017); vi) moving cargo or actin filaments; and vii) F-actin anchoring-proteins that anchor actin filaments to other cellular compartments. Due to interaction with ABPs, actin can be a multipotent protein participating in several and distinct roles of the cell. During this thesis, we will focus our attention in Arp2/3 and formins, that catalyse the nucleation and elongation of F-actin.

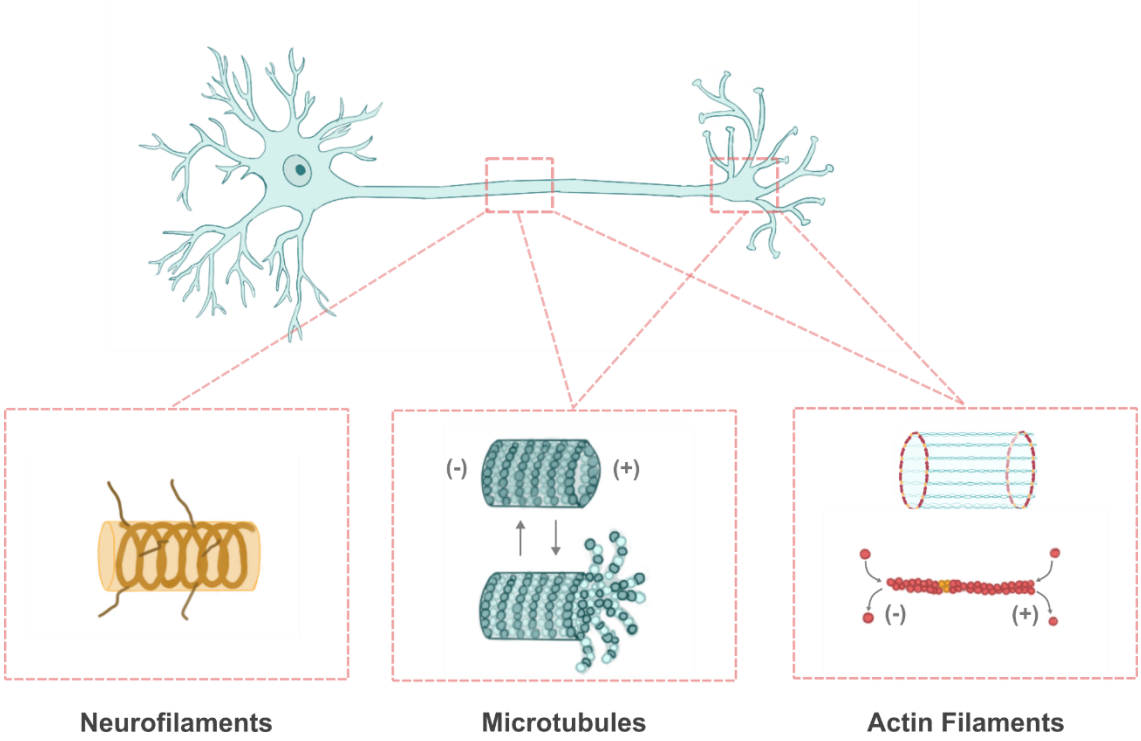

Figure 4 – Schematic representation of the three mains constituents of the cytoskeleton: neurofilaments, microtubules and actin filaments. Both microtubules and actin filaments are distributed through the axon and growth cone, while neurofilaments are found in the axon.

3.3.1 The Arp2/3 Complex

Actin polymerisation can occur spontaneously. During this process, the addition of monomers to the end of a preexisting filament (elongation) is energetically more favourable than the addition of monomers to form a new filament (nucleation). To overcome this kinetic barrier, Arp2/3 has a significant role. Arp2/3 was initially identified in 1994 when Pollard's laboratory searched for molecules binding to profilin, an ABP. Using poly-L-proline Sepharose affinity columns, able to bind recombinant profilin, a seven-component complex was isolated (Schroer et al., 1994), being two of the subunits identified as "unconventional" actins, due to their similarity with actin: Arp2 and Arp3. The seven-component complex was then named Arp 2/3. The Arp2/3 complex is evolutionarily conserved from yeast to humans and it is present as a seven-subunit complex: Arp2, Arp3 and Arp2/3 complexes 1-5 (ARPC1-5) (Cooper et al., 2001; Dayel & Mullins, 2004; Egile et al., 2005; Goley & Welch, 2006; Padrick et al., 2011; Pizarro-Cerdá et al., 2017; Rouiller et al., 2008). Its impact on actin polymerization is critical, as it generates branched actin networks at 70º of the mother filament. Arp2/3 plays a pivotal role in cell migration, triggered by lamellipodia, endocytosis, and the formation of clathrin-coated pits for the internalization of extracellular materials. Moreover, in the context of

cytokinesis, the Arp2/3 complex assumes a crucial role by assembling a contractile ring that facilitates the separation of daughter cells while also regulating the kinetics to prevent excessive activity of formins. These examples illustrate the versatility and irreplaceable nature of this complex (Chan et al., 2019; Goley & Welch, 2006; Pizarro-Cerdá et al., 2017).

Regulation and Activation of the Arp2/3 Complex

The activity of the Arp2/3 complex (Figure 5), which is a critical regulator of actin cytoskeleton dynamics, is subject to multifaceted regulation. The structural arrangement represents the inactive state since the Arp2/3 complex alone shows reduced or no activity. Several key factors govern its function, including nucleotide binding and hydrolysis by Arp2 and Arp3, phosphorylation of the complex and its subunits, and interaction with NPFs. Particularly, the Arp2 and Arp3 subunits each exhibit a micromolar affinity for ATP, and any mutations diminishing this affinity in either Arp subunit result in a significant reduction in complex activity (Cooper et al., 2001; Dayel & Mullins, 2004; Goley & Welch, 2006; Padrick et al., 2011).

As previously mentioned, activation of the Arp2/3 complex relies largely on the action of nucleation-promoting factors (NPFs). Several classes of NPFs, such as Wiskotl-Aldrich Syndrome Protein (WASP) family proteins, Wasp- Family Verprolin- Homologous Protein (WAVE) family proteins, and WASP homologue-associated protein with actin, membranes and microtubules (WHAMM) family proteins, exert their influence on the complex through distinct structural and mechanistic pathways. The activation of the Arp2/3 complex involves the addition of the first subunit of the new filament by a WASP protein. This triggers rapid ATP hydrolysis on Arp2, with no detectable lag phase. When ATP binds to Arp3, it induces a conformational change within the complex by closing its nucleotide-binding cleft, which is indispensable for its activation. Furthermore, the activity of the Arp2/3 complex is regulated by upstream signaling pathways, particularly those involving Rho GTPases. These pathways activate NPFs, which in turn facilitate the recruitment of the Arp2/3 complex to specific subcellular locations (Dayel & Mullins, 2004; Padrick et al., 2011). Once activated, the Arp2/3 complex attaches to the side of an existing actin filament (called “mother filament”), effectively initiating branch formation (called “daughter filament”) at a precise 70-degree angle (Figure 5). To maintain precise control over this process and prevent untimely branch nucleation, specific regulation is mediated by various factors, including actin-binding proteins, signaling molecules, and other interacting proteins. This intricate network of regulatory mechanisms ensures the precise and dynamic control of Arp2/3 complex activity in the actin cytoskeleton (Amann

& Pollard, 2001; Cooper et al., 2001; Dayel & Mullins, 2004; Padrick et al., 2011; Smith et al., 2013).

Subunit organization and structure

When dissecting the roles of Arp2/3 complex, it is essential to understand the distinct roles of the individual subunits. Arp2 and Arp3, structurally similar to actin, comprise the core of the complex, being able to bind the existing actin filaments ("mother" filament) and catalyse the creation of new branches. They are folded like actin and form the first two subunits of the daughter filament (Cooper et al., 2001; Dayel & Mullins, 2004; Egile et al., 2005; Goley & Welch, 2006; Padrick et al., 2011; Pizarro-Cerdá et al., 2017; Rouiller et al., 2008). Despite ARPC1 having limited direct interaction with the mother actin filament, due to basic residues exposed to the surface, it interacts with other subunits within the complex and NPFs, activators of Arp2/3, to ensure the development of branched actin filament networks. Notably, this subunit is the largest in the complex and it is believed to play a role in regulating its activity. It possesses several domains capable of interacting with other proteins, including a BAR domain that binds to membranes. ARPC2 stabilizes the interaction between Arp2 and Arp3 while also facilitating the interaction with other proteins. On the other hand, ARPC3 acts as a bridge between Arp3 and the mother actin filament, thus enhancing nucleation efficiency. Interestingly, the deficiency of ARPC3 results in relatively minor functional defects. ARPC4 and ARPC5 similarly participate in the complex's activity regulation, ensuring its proper functioning. A dimer comprising ARPC2 and ARPC4 forms the structural backbone of the complex, facilitating interaction with the mother actin filament. Lastly, ARPC5 is proposed to anchor Arp2 to the rest of the complex. In conclusion, understanding the distinct roles of the individual subunits within the Arp2/3 complex is crucial when dissecting its functions (Cooper et al., 2001; Goley & Welch, 2006; Padrick et al., 2011; Pizarro-Cerdá et al., 2017).

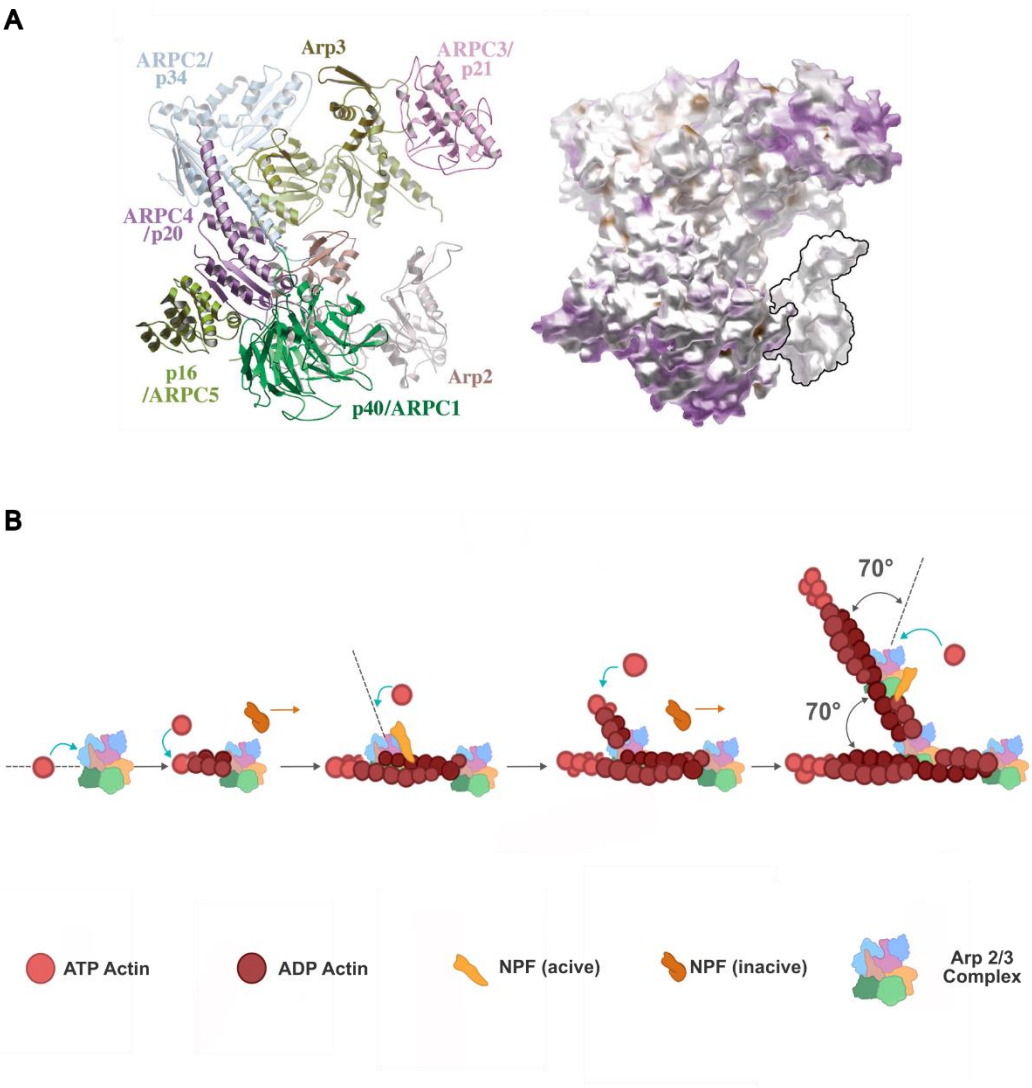

Figure 5- Schematic representations of the Arp 2/3 complex structure and mechanism of action. A. Crystal structure of the Arp 2/3 complex composed of seven subunits: Arp2, Arp3, ARPC1/p40, ARPC2/p34, ARPC3/p21, ARPC4/p20 and ARPC5/p16. Adapted from (Cooper, Wear, & Weaver, 2001). **B.** Illustration of the mechanism of action of the Arp 2/3 complex. The Arp 2/3 complex coordinates the anchor of the new filament's pointed end to the existing actin network at an approximate 70° angle, the NPFs facilitate the transportation of actin monomers to the Arp2/3 complex at the barbed end, by binding through their WH2 domain. This interaction facilitates the generation of new filament branches from the sides of pre-existing filaments.

3.3.2 Formins

Polar actin filaments have a slow-growing "pointed" end, or “minus” tip, and a fast-growing "barbed" end, or “plus” tip. Generally, in cells, actin filaments extend from the barbed end of actin. Therefore, nucleators associated with pointed ends, such as Arp2/3, are unsuitable for generating long actin filaments. In this particular case, capping proteins bind rapidly to the free-barbed ends, thus blocking the addition of monomers and hindering the formation of extended actin filaments. Previously, we explored the nucleation of small filaments of actin, but large ones are also found in the axonal cytoskeleton. Importantly, formins have emerged as pivotal contributors to actin

cytoskeletal dynamics by facilitating both filament nucleation and elongation (Figure 6) (Chalkia et al., 2008; Courtemanche, 2018; Evangelista et al., 2003; Goode & Eck, 2007; Higgs, 2005; Kovar, 2006; Moseley et al., 2006; Paul & Pollard, 2009). Formins are a multi-domain family of fifteen proteins of more than 140 kDa in weight, and including in its structure the conserved domains: formin homology 1 (FH1) and 2 (FH2) (reviewed in Innocenti, 2023) (Higgs, 2005; Kovar, 2006). The FH2 domain binds directly to actin monomers and filaments, thus participating in their nucleation and elongation. FH2 is a long domain comprising approximately 400 residues, and it forms a doughnut-shaped head-to-tail dimer that remains associated with the barbed end of the filament. Hence, the binding of capping proteins during elongation is prevented. A proline-rich domain, FH1, precedes FH2. This domain is able to interact with profilin for the recruitment of monomeric actin, thus accelerating the actin polymerization rate. Profilin is a small ABP that binds to actin monomers and promotes their rapid addition to growing filaments. The FH1 domain binds to profilin-actin complexes and delivers them to the FH2 domain, where they are added to the growing filament. Both domains work together to facilitate actin filament assembly. Other domains that are commonly found in formins include the GTPase-binding domain (GBD), the diaphanous inhibitory domain (DID), the dimerization domain (DD), the coiled coil region (CC), and the diaphanous autoinhibitory domain (DAD). These domains are involved in regulating the activity of formins and controlling its interactions with other proteins and signalling pathways (Evangelista et al., 2003; Gaillard et al., 2011; Goode & Eck, 2007; Paul & Pollard, 2009; Yang et al., 2007). These proteins have been implicated in several developmental and homeostatic cellular processes such as signalling, mitochondrial fission, trafficking of vesicles and organelles, membrane protrusion, endocytic pathways, in the establishment and maintenance of polarity for cell division, and cell migration (reviewed in Innocenti 2023) (Evangelista et al., 2003; Gaillard et al., 2011; Goode & Eck, 2007; Higgs, 2005; Kovar, 2006; Moseley et al., 2006; Paul & Pollard, 2009), by remodelling the actin cytoskeleton.

Diaphanous-related formins (DRFs), are a subset of formins including the four mammalian families mDia, Daam, FMNL, and FHOD, that are autoinhibited and regulated by Rho GTPases. In the resting state, an intramolecular interaction between the DAD domain and its DID domain occurs, causing its autoinhibition, which is reverted by the binding of Rho GTPase, such as Rho, Rac, or Cdc42, through the N-terminal of the GBD. Since, in this thesis we will focus our attention in mDia1 and mDia2 and their role in the axon cytoskeleton, we will briefly explore both proteins.

mDia1

mDia1, is a member of the formins family, and plays an important role in the complex dynamics of actin and microtubule cytoskeleton within cells. It interacts with both microtubules and actin filaments and is essential for reorientation of the microtubule organizing center in T cells during interactions with antigen-presenting cells. This pivotal role ensures the proper communication and coordination of the immune response. The influence of mDia1 extends beyond the immune response. It actively participates in the regulation of cell migration, cytokinesis, and cell polarity, contributing to the fundamental processes that shape the development and maintenance of tissues and organs. Regarding its role in neurons, a previous study confirmed that mDia1 is the primary target of SMIFH2, a general inhibitor of formins activity (Qu Xiaoyi and Bartolllini, et al., 2017). Moreover, mDia1 modulates axonal and dendritic structures (Qu Xiaoyi and Bartolllini, et al., 2017). When dysregulated, mDia1 is implicated in various diseases, including cancer and developmental disorders, underlining its significance in maintaining cellular homeostasis. (Gaillard et al., 2011; Goh & Ahmed, 2012; Maiti et al., 2012; Nezami et al., 2006).

One distinguishing feature of mDia1 is its remarkable ability to tightly couple helical rotation with actin elongation. This unique capability is achieved by the regulation of actin filament nucleation and elongation. Moreover, mDia1 interacts with an array of other proteins and signalling pathways, including Rho GTPases and the Wnt signalling pathway, to modulate cellular processes. mDia1 structure comprises a Rho binding domain (RBD) in its N-terminus and anchors itself to the plasma membrane by binding to regulatory proteins, such as anillin and liprin α. Visualization of this coupling process through single-molecule fluorescence polarization has been a groundbreaking revelation in understanding the mechanisms underlying mDia1 and formins' control over actin filament elongation and stability (Gaillard et al., 2011; Maiti et al., 2012; Mizuno et al., 2011; Tominaga et al., 2000).

Furthermore, the interaction between mDia1 and profilin has unveiled intriguing insights. Profilin accelerates the depolymerization of ADP-F-actin bound to mDia1, revealing the counterbalancing effects of ATP and ADP-actin on the rate of filament elongation catalysed by formins and profilin. These discoveries have enriched our understanding of the intricate dynamics governing actin filaments within the cells. mDia1's influence extends beyond actin regulation. As previously mentioned, it interfaces with the microtubules, affecting their stability and dynamics. This protein encompasses the FH1 and FH2 domains, which participate in actin nucleation and elongation, respectively. This dual functionality further underscores its versatility in

cytoskeleton control. (Jégou et al., 2013; Maiti et al., 2012; Nezami et al., 2006; Pollard, 2011; Yu et al., 2017)

mDia2

Another member of the formins family, mDia2, similarly to mDia1, is involved in the dynamics of actin and microtubule cytoskeleton within cells. Similarly to mDia1, mDia2 is a versatile player that influences processes, such as cell migration, cytokinesis, and cell polarity. However, mDia2 distinguishes itself by having a particular role on cytokinesis, where it plays a pivotal role in the formation and stabilization of the contractile ring during cell division. Within its structure, mDia2 harbours FH1 and FH2 domains, specializing in actin nucleation and elongation. Beyond actin, mDia2 extends its reach to microtubules through the C-terminal region, where it acts as a regulator of its stability and dynamics. (Bartolini et al., 2008; Goh & Ahmed, 2012; Mei et al., 2020)
Beyond its conventional roles, mDia2 has been implicated in the complex world of neuronal development and function. It is involved in the formation and maintenance of dendritic spines, critical structures for synaptic transmission, and plasticity in neurons. Additionally, mDia2 plays a role in the regulation of axon guidance and growth cone dynamics. These processes are vital for intricate wiring and rewiring of the nervous system, underscoring mDia2's significance in the field of neuroscience. Depletion of mDia2 has been shown to diminish the rate and persistence of lamellipodia protrusion, impairing cell migration. Additionally, mDia2's influence extends to membrane trafficking and transcription processes. Its versatility in orchestrating actin and microtubule dynamics, coupled with its novel role in neuronal development and function, underscores its importance in cellular physiology and pathology (Bartolini et al., 2008; Chesarone et al., 2010; Gaillard et al., 2011; Goh & Ahmed, 2012; Mei et al., 2020; Yang et al., 2007).

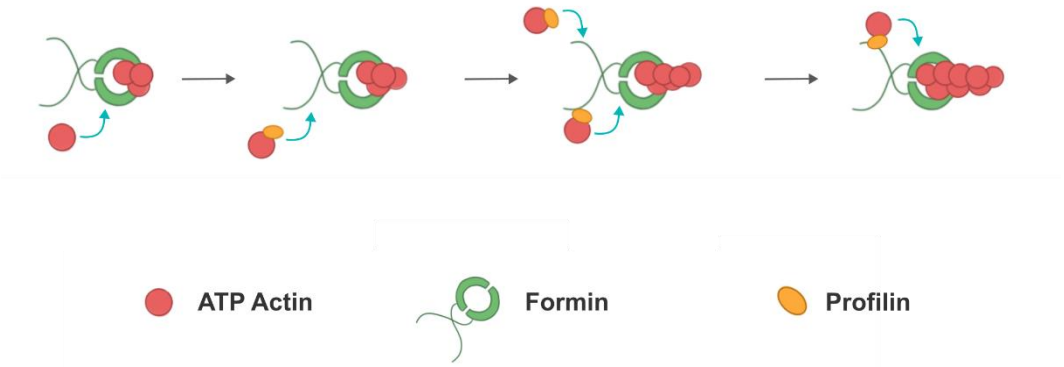

Figure 6 - Schematic representation of formins' mechanism of action. Formins dimers (in green), promote the initiation of filament assembly by binding to actin monomers through their FH2 domains and they facilitate elongation of existing filaments by removing barbed end capping proteins while forming a protective sleeve around the actin subunits.

4. The Membrane Periodic Skeleton (MPS)

The development of super-resolution microscopy contributed to better characterizing the cell´s ultrastructure. So far, the most striking new structure identified by nanoscopy is the axonal membrane periodic skeleton (MPS). The MPS is a complex neuronal structure characterized by the arrangement of actin into rings evenly spaced along the axon, typically at intervals of about 190 nanometers (Figure 7) (Costa & Sousa, 2021; Costa et al., 2020; Leite & Sousa, 2016; Xu et al., 2013; Zhong et al., 2014). The MPS emerges early during axon development in cultured hippocampal neurons and propagates from proximal regions to distal axonal ends (Costa & Sousa, 2021). The MPS is present in every neuron type inspected so far either belonging to the CNS or PNS (D'Este et al., 2015; He et al., 2016; Leite et al., 2016a; Lukinavicius et al., 2014; Xu et al., 2013; Zhong et al., 2014), and in a small fraction of dendrites (D'Este et al., 2016; Zhong et al., 2014). Similarly to unmyelinated axons in the CNS, myelinated sciatic nerve axons contain the periodic lattice (D'Este et al., 2016). Within the nervous system, the MPS might not be exclusive of neurons as the processes of different glial cell types including astrocytes, microglia, NG2 glia, Schwann cells and oligodendrocytes show patches of a similar periodic skeleton (D'Este et al., 2016; Hauser et al., 2018; Zhong et al., 2014). This unique arrangement of the cytoskeleton is observed in axons across species, from invertebrates (*C. elegans* and *D. melanogaster* (He et al., 2016)) to vertebrates (chicken (He et al., 2016), mice, rats (D'Este et al., 2016; He et al., 2016; Lukinavicius et al., 2014; Xu et al., 2013; Zhong et al., 2014) and humans (He et al., 2016)), supporting its importance for neuronal function.

While the membrane periodic skeleton (MPS) exhibits a unique ultrastructure and

arrangement, it shares some structural components with the erythrocyte membrane-cortical cytoskeleton (EMCC) (Nicolas Unsain et al., 2018; Wang et al., 2019). As such, tetramers of spectrin connect the MPS actin rings (Xu et al., 2013). Spectrins are large flexible molecules that are mainly present as heterotetramers of α and β subunits, formed upon the arrangement head-to-head of antiparallel α/β dimers (Bennett et al., 1982; Shotton et al., 1979). In axons, αII/βIV-spectrin is found proximally to the cell body in the AIS (Galiano et al., 2012), whereas αII/βII-spectrin is enriched in the remaining axon shaft (Galiano et al., 2012), and αII/βIII-spectrin is mostly observed in dendrites (Stankewich et al., 2010). Although βIV and βII spectrins present a periodic pattern within the AIS and axon shaft, respectively, the regular lattice is detected only in small patches in dendrites (D'Este et al., 2015; Han et al., 2017; Zhong et al., 2014). Beyond actin, spectrin, ion channels (Xu et al., 2013), and adducin (Leite et al., 2016a), an actin-binding protein capping the actin barbed end, an expanding array of associated proteins emerges, such as non-muscle myosin II (NMII) (Berger et al., 2018; Costa et al., 2020; Wang et al., 2020) and tropomyosin 3.1 (Abouelezz et al., 2020). Moreover, the use of state-of-the-art biochemical approaches (Hamdan et al., 2020; Zhou et al., 2020; Zhou et al., 2019) allowed the identification of several MPS proteins. Specifically, with co-immunoprecipitation and mass spectrometry, hundreds of candidate MPS-interacting proteins were found including motor proteins, cell adhesion molecules, ion channels, and signaling molecules (Zhou et al., 2020). Determining the MPS proteome is essential to further comprehend its function(s) in neuronal biology. Since its initial identification, the contribution of the MPS to the integrity and mechanical stability of the axon has been widely accepted (Dubey et al., 2020; Rief et al., 1999; Zhang et al., 2019). With the identification of more components belonging to this structure, additional aspects of neuronal physiology are currently emerging. This includes the formation and function of the AIS (Albrecht et al., 2016; Berger et al., 2018; D'Este et al., 2017; Huang et al., 2017; Zhong et al., 2014), the regulation of axon diameter (Costa et al., 2020; Leite et al., 2016a; Wang et al., 2020) in the course of action potential conduction (Costa et al., 2020) and axonal transport (Wang et al., 2020), and the modulation of the stability of axonal microtubules (Y. Qu et al., 2017). Disruption of the MPS causes widespread neurodegeneration (N. Unsain et al., 2018; Wang et al., 2019) and a variety of neurological impairments are seen when its components are mutated and downregulated (Gallardo et al., 2014; Kruer et al., 2013; Leite et al., 2016a).

Based on adducin capping properties, the MPS was initially proposed to be organized as short actin filaments (Xu et al., 2013). Later, combining platinum-replica electron and optical super-resolution microscopy, the MPS actin rings were proposed to

present two long intertwined actin filaments (S. Vassilopoulos et al., 2019), where adducin would enhance the lateral binding of spectrin to actin (S. Vassilopoulos et al., 2019), instead of capping actin filaments. The braided actin arrangement was suggested to provide more stability to the structure, as it is expected to be stiffer than a ring made of short actin filaments (S. Vassilopoulos et al., 2019). Further experiments are needed to fully understand how actin is nucleated in the MPS, which is the main aim of this thesis. Based on their effects on actin polymerization, we intend to investigate if Arp2/3 and/or the formins, mDia1 and mDia2, are important for MPS formation and maintenance.

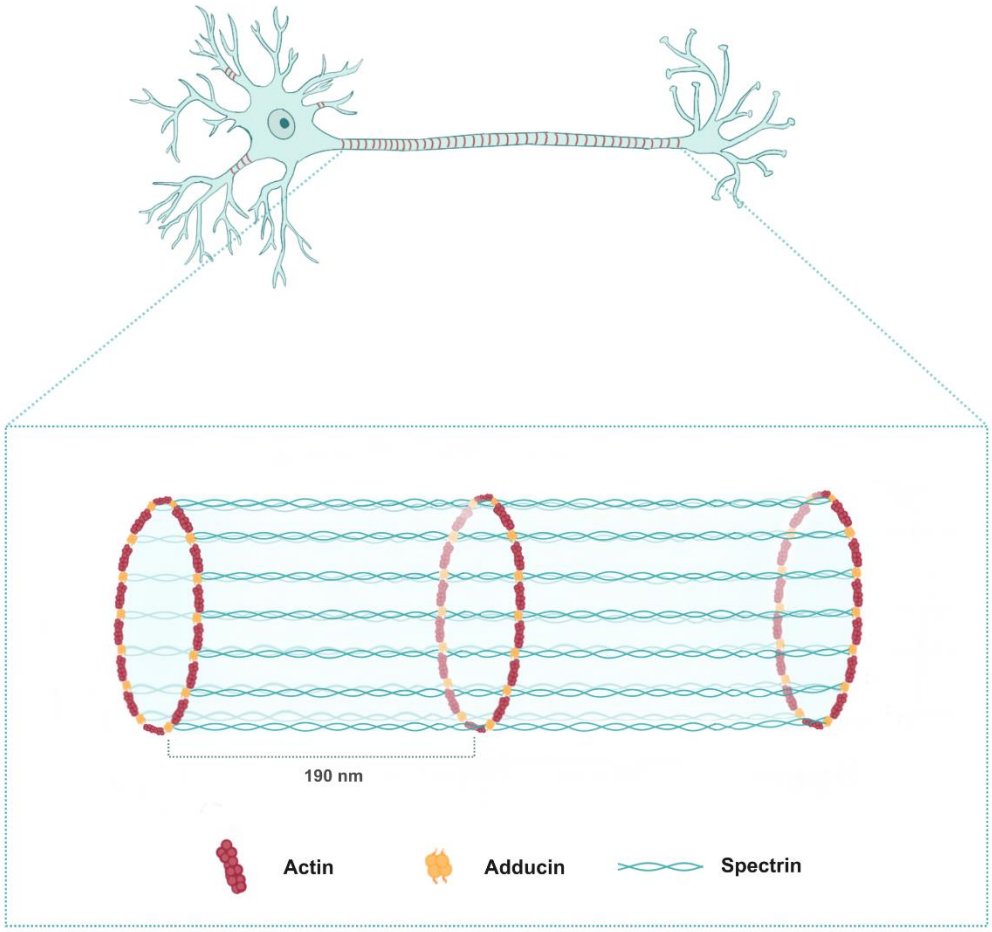

Figure 7 - Schematic illustration of the membrane-associated periodic skeleton (MPS) of neurons and its associated proteins. The MPS is composed of actin rings evenly spaced by spectrin occurring periodically every 190 nanometers throughout the entire length of the axon. The actin rings are composed by filaments of actin capped by adducin. The MPS can also be found in some dendrites.

Objectives

The main goal of our research is to unravel the mechanisms underlying axonal MPS biogenesis, maintenance and function, focusing particularly on the mechanisms involved in actin ring nucleation and the dynamic nature of their formation and maintenance. For that, the role of different actin nucleators, Arp2/3 and formins, will be investigated and the following objectives were proposed:

I. Determine the effect of CK869 and SMIFH2, specific drug inhibitors of Arp2/3 and formins, respectively, in cell morphology and on the formation and maintenance of the MPS;
II. Abolish the expression of Arp2/3 by using the genetic tool CRISPR-Cas9 and evaluate its effect on the formation and maintenance of the MPS;
III. Reduce formins expression by using shRNA against mDia1 and mDia2 and evaluate their effect on MPS formation and maintenance.

By attaining these objectives, a more comprehensive knowledge of the mechanisms governing MPS actin ring development and maintenance is expected.

Material and Methods

1. Animals

All animal procedures strictly adhered to both the national Decreto-lei no. 113-2013 and the European Union Directive 2010/63/EU regulations. Each animal was bred and housed within the i3S animal facility, where they were provided with unrestricted access to standard rodent food and water. Environmental conditions were maintained at 20 to 24 °C, with a 12-hour light and dark cycle, while the humidity level was carefully maintained at 45–65%. Pregnant Wistar female rats at embryonic day 18 (E18) were euthanized using a CO_2 chamber, following the recommended procedures outlined by the animal facility guidelines.

2. Primary Neuron Cultures

2.1 Coatings

Prior to the Hippocampal Neuron Culture, the 24 well plates with 1.5H glass 13 mm rounded coverslips (Marienfeld, for STED imaging, #0117530) were coated with 50 mg/mL poly-L-lysine (PLL) hydrobromide (Sigma-Aldrich, #P2636-100MG). For this, one coverslip was placed in each well and the 24 well plate was taken to the Plasma Cleaner (Tergeo Plasma Cleaner, Pie Scientific (TG100)). The following protocol was applied: Air channel, at a power of 75 W for 1 minute and 30 secs. After that, the plate was incubated with 500 µL of PLL per well for 1 hour at 37°C in a 5% CO2 incubator. Finally, the wells must be washed two times with 1x PBS.

2.2 Hippocampal Neuron Cultures

Hippocampal cultures were established following an adapted version of the Kaech and Banker protocol (Kaech & Banker 2006). Pregnant rat females at E18 were euthanized per established guidelines, and the embryos were carefully removed to extract the hippocampi. Hank's balanced salt solution (HBSS, Sigma-Aldrich, #H9394-1L) in ice was utilized to ensure optimal preservation of the dissected hippocampi.

After washing three times with HBSS, a 15-minute enzymatic treatment with 0.06% porcine trypsin (Sigma Aldrich, #9002-07-7) was applied to the hippocampi at 37°C in a 5% CO_2 incubator. Subsequently, 10 mL of 10% FBS (Sigma Aldrich, # F9665-500ML) were added to stop trypsin's activity. In addition to the chemical dissociation, a mechanical dissociation was performed to the tissue pellet by resuspending it in 1 mL of Neurobasal medium (Invitrogen, # 21103-049) supplemented with 1x B-27 (B-27 supplement (50X), Invitrogen, #17504044), 1% Penicillin/Streptomycin (P/S, 10,000 U/mL Gibco™, #15140-122) and 2 mM L-Glutamine (L-glu, Thermo Scientific™, #25030024) using a 1000 µL pipette tip followed by a 200 µL pipette tip. The resulting solution was then filtered through a 70 µm cell strainer to ensure the removal of any remaining undissociated tissue. Cells were counted in a Neubauer chamber (VWR International, #631-0696). Initially, 10 µL of the filtered cell solution were diluted in 90 µL of the supplemented neurobasal medium, followed by a 1:1 dilution with trypan blue 0.4% (Sigma-Aldrich, #T8154). After counting, cells were plated onto pre-coated coverslips. Both 24- or 6-well plates (VWR (Corning), # 734-1606 (CORN3527) and # 734-1596 / CORN3506) were used, and different densities were plated depending on the specific experimental objectives and requirements. For transfections, 50,000 cells were plated per well in a 24-well plate, while for drug administration, 25,000 cells were plated per well in a 24-well plate. Throughout the experiment, cells were maintained at 37°C under a 5% CO2 atmosphere in the incubator until the desired day in vitro (DIV).

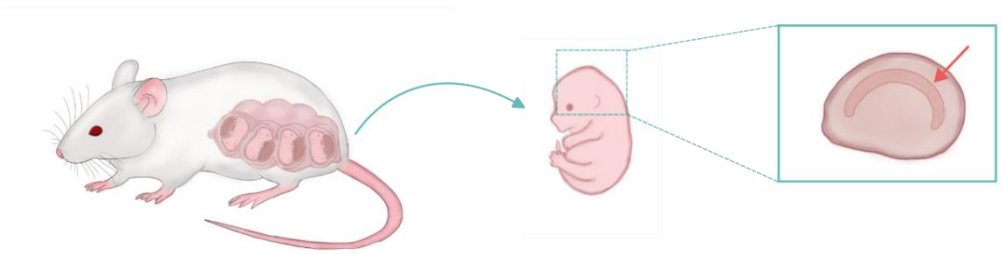

Figure 8 – Schematic representation of the of the steps involved in the dissection of hippocampal neurons. At E18, pregnant rat females were euthanized, the embryos were carefully removed and the hippocampi were extracted.

3. Cell Line Culture

To further validate our genetic approaches, a cell line was used. Various cell lines were tested, including PC-12 and RN-22 and rat fibroblasts isolated from lungs before identifying the optimal one for our intended applications, RAT-2 (ATCC, #CRL-1764), a rat fibroblast cell line. Upon their arrival, the cells were suspended in complete cell media,

consisting of Dulbecco's Modified Eagle Medium (DMEM) High Glucose (Capricorn Scientific, #DMEM-HA) supplemented with 10% FBS (Sigma Aldrich, # F9665-500ML) and 1% Penicillin-Streptomycin (P/S, 10,000 U/mL Gibco™, #15140-122), within a T25 flask (VWR, #734-1712). Once reaching 70-80% confluency, the cells were transferred to a T75 flask (Sarstedt, #83.3911.002). When the cells were intended to use in transfections, the cells were counted using a Neubauer chamber (VWR International, #631-0696). For this, after adding the 4 mL of the cell complete media to the 2 mL suspension of cells in trypsin (Trypsin 0,05% EDTA (1X), Alfagene, #25300062), cells were centrifuged at 1000 RPMs for 5 minutes. Then the cell pellet was resuspended in 5 mL of the cells' complete media. A 1:1 dilution with trypan blue 0.4% (Sigma-Aldrich, #T8154) and cell counting was performed. A density of 50,000 cells per well was plated in 24 well plates and stored at 37°C under a 5% CO2 atmosphere.

4. Drugs

Two different chemical drugs were used: CK689, inhibiting actin polymerization of Arp2/3 and SMIFH2 inhibiting the linear polymerization of actin by formins.

4.1 CK869

CK869 (Sigma-Aldrich, # C9124-5MG) was added acutely at DIV 5 and DIV14 one hour preceding its fixation. A stock solution of 25 mM (DMSO (Sigma-Aldrich, #D4540) is used to prepared a final concentration of 10 µM.

4.2 SMIFH2

SMIFH2 (Scientific Laboratory Supplies, # S4826-5MG) was added acutely at DIV 5 and 14. On the day of drug administration, the 24-well plate was retrieved from the incubator, and a solution of 25 µM of SMIFH2 diluted in 500 µL of the cells' complete media was added to each well. After 30 minutes the cells were fixed.

5. Immunocytochemistry

After removing the complete media, cells were fixed using 4% paraformaldehyde (PFA, Sigma-Aldrich, #158127-500G) for 10 minutes at room-temperature (RT). At this point, 500 µL of PBS with 0.1% Azide (Sigma-Aldrich, #S2002-25G) was added and the fixed coverslips were stored at 4°C for later use, or the next step of the protocol would be done. Afterwards, each coverslip was washed three times with PBS to remove any

residual solutions or debris. In order to permeabilize the cell membranes, a brief 3-minute incubation with 0.1% Triton X-100 in PBS (Sigma-Aldrich, #T9284-100ML) was performed, followed by an additional PBS wash. To effectively reduce autofluorescence, the samples were then subjected to a 3-minute incubation with NH4Cl (200mM prepared in water) (VWR (Merck), #1.01145.0500). For blocking purposes, the cells were treated with a 5% FBS (Sigma Aldrich, # F9665-500ML) in PBS solution and incubated for 30 minutes at 37°C. The coverslips were carefully removed from the wells and placed in a petri dish lined with filter paper soaked in water and parafilm. The primary antibody (Table 1) solution was added to each coverslip (50 µL per coverslip) and left over-night (ON) at 4°C. On the subsequent day, following three washes with PBS the secondary antibody (Table 2) solution was added and incubated for 30 minutes at 37 °C. For STED samples, after the incubation with the secondary antibody and a three-time wash with PBS, a solution of phalloidin (Abberior STAR 635, # ST635) was added to each coverslip for 30 minutes at 37°C. To mount the coverslips onto microscope slides, either DAPI mounting solution or a glycerol mounting media was utilized, and the process was completed by sealing the coverslips with clear nail polish.

Table 1 - List of the Primary Antibodies used for Immunocytochemistry.

Primary Antibody	Target	Dilution	Source
Phospho-Myosin Light Chain 2 (Thr18/Ser19) Rabbit Ab	Rabbit	1:50	Cell Signaling Technology/ #3674
mDia1	Mouse	1:50	BD Transduction Laboratories™/ #610848
Anti-β-Spectrin II	Mouse	1:50	BD Transduction Laboratories™/ #612562
p34-ARC	Mouse	1:50	SYSY/ #306 011
P16-ARC	Mouse	1:50	Santa Cruz/ #sc-166760
DIAPH3 Rabbit PolyAb	Rabbit	1:50	Proteintech/ #14342-1AP
Anti-βIII Tubulin mAb	Mouse	1:50	Promega/ #G712A

Table 2 - List of the Secondary Antibodies used for Immunocytochemistry.

Secondary Antibody	Target	Dilution	Source
Donkey Anti-Rabbit IgG Antibody (Alexa Fluor® 488)	Rabbit	1:200	Jackson ImmunoResearch/ #711-545-152
Abberior STAR 580	Mouse	1:200	Abberior/ #ST580
Alexa Fluor 594-conjugated affinipure donkey anti-mouse IgG	Mouse	1:200	Jackson ImmunoResearch/ #715-585-150

6. Neurite Outgrowth Evaluation

The neurons treated with drugs were used for neurite outgrowth assessment using immunofluorescence (protocol above described). Imaging was conducted using Leica DMI6000 FFW microscope (at the i3s' Advanced Light Microscopy facility). The images were captured with a 20x objective, using the filters: Alexa Fluor 488, and 594 and merging the images encompassing the entire area of the coverslip. Neurite tracing was subsequently executed utilizing the ImageJ software along with the NeuronJ plugin. Both axon and dendrite length were evaluated.

7. Plasmids

Cells were transfected using five different conditions, two of them specific to the Arp2/3 experiment and three specific to the formin experiment.

7.1 Conditions and Plasmids used for the Arp2/3 experiment

For the Arp2/3 experiment three different conditions were used:

1) A control using co-transfection of a plasmid expressing Cas9 (VB220503-1078vkb plasmid; pRP[Exp]-Puro-CBh>hCas9; from Vectorbuilder- Figure 9 under the promoter CBh followed by puromycin resistance under the CMV promoter) and a plasmid expressing a guide targeting the locus ROSA26: VB220418-1131hns plasmid (pRP[gRNA]-EGFP-U6>{guideRNA

control_ROSA26}; from Vectorbuilder; Figure10) under the promoter U6 followed by eGFP under the promoter hPGK. The guide RNA for the genomic locus of interest (5'-GCAGATCACGAGGGAAGAAG-3') was designed using Vectorbuilder based on the sequenced ROSA26 locus from Wistar rats.

2) A experimental condition in which RAT-2 cells or hippocampal neurons were co-transfected with the previously described CRISPR-Cas9 vector (pRP[Exp]-Puro-CBh>hCas9; from Vectorbuilder) (Figure 9) and a plasmid expressing the guideRNA for the exon2 of the ARPC2 subunit of Arp2/3: VB220503-1078vkb plasmid (pRP[gRNA]-EGFP-U6>{ARPC2}; from Vectorbuilder) (Figure 11) under the promoter U6 followed by eGFP under the promoter hPGK. The guideRNA for the genomic locus of interest (5'-CCCAGTGTGCGCTTACCCGG-3') was designed using Vectorbuilder based on sequenced ARPC2 from Wistar rats.

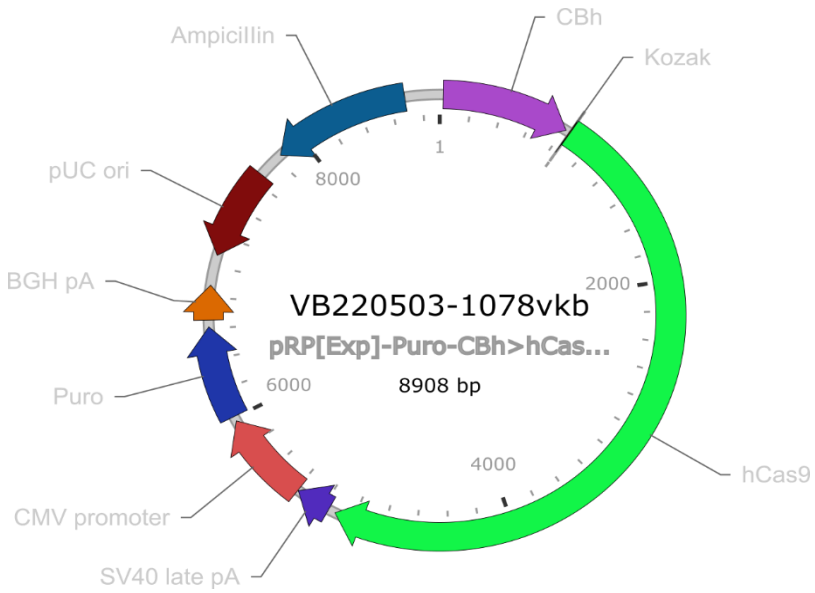

Figure 9- Map of the VB220503-107vkb plasmid expressing CRISPR-Cas9 (pRP[Exp]-Puro-CBh>hCas9; from Vectorbuilder. Cas 9 is expressed under the promoter CBh followed by puromycin resistance under the CMV promoter.

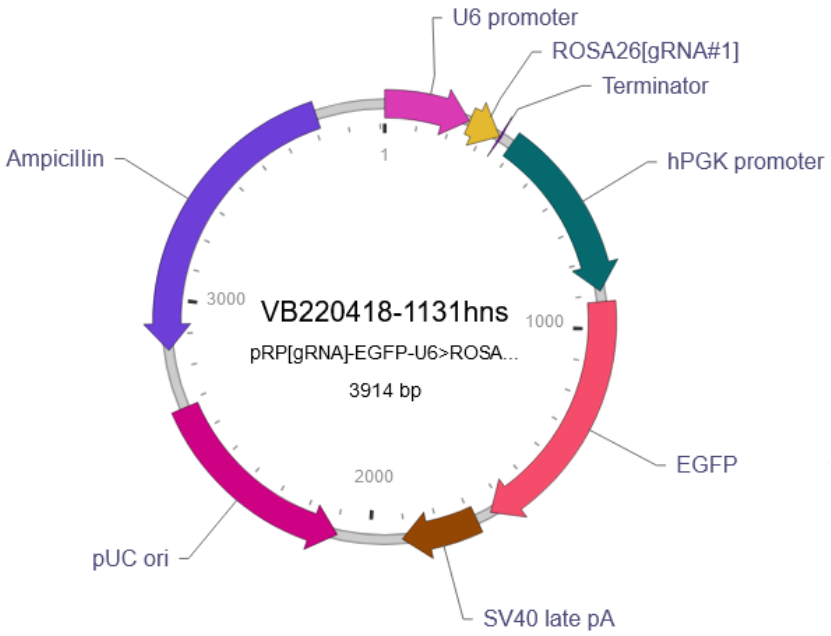

Figure 10 – Map of the VB220418-1131hns plasmid expressing a guide targeting the locus ROSA26: (pRP[gRNA]-EGFP-U6>{guideRNA control_ROSA26}; from Vectorbuilder**. The guide is expressed** under the promoter U6 followed by eGFP under the promoter hPGK.

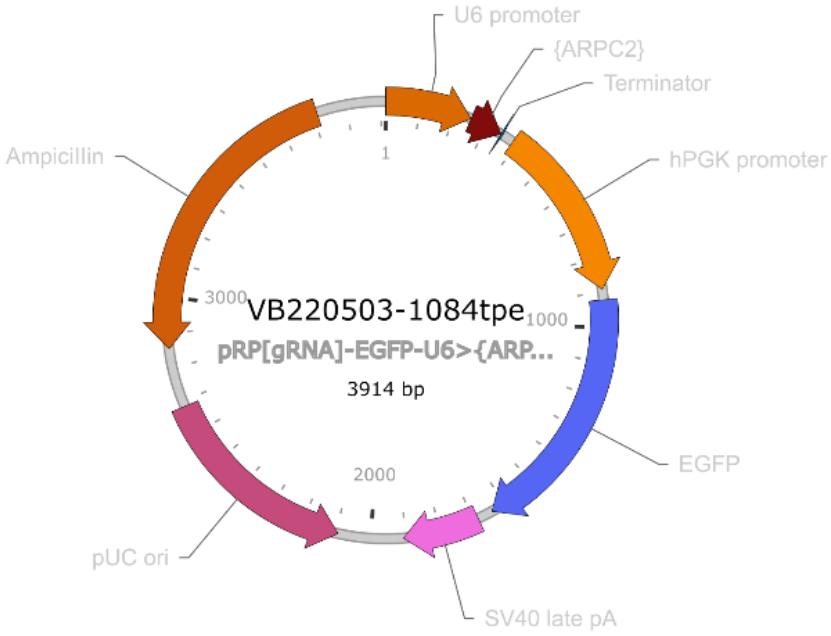

Figure 11 – Map of the VB220503-1078vkb plasmid expressing the guideRNA for the exon2 of the ARPC2 subunit of Arp2/3 (pRP[gRNA]-EGFP-U6>{ARPC2}; from Vectorbuilder). The guide RNA is expressed under the promoter U6 followed by eGFP under the promoter hPGK.

7.2 Conditions and Plasmids used for the formin experiment

For the formin experiment three different conditions were prepared:

1) A <u>control condition</u> using the pLKO.1-TRC control plasmid (Figure 13) co-transfected with pEGFP-c1 plasmid (from Clontech). The pLKO.1-TRC control was a gift from David Root (Broad Institute) (Addgene plasmid # 10879; RRID:Addgene_10879). This plasmid includes a U6 promoter and puromycin resistance under the hPGK promoter.

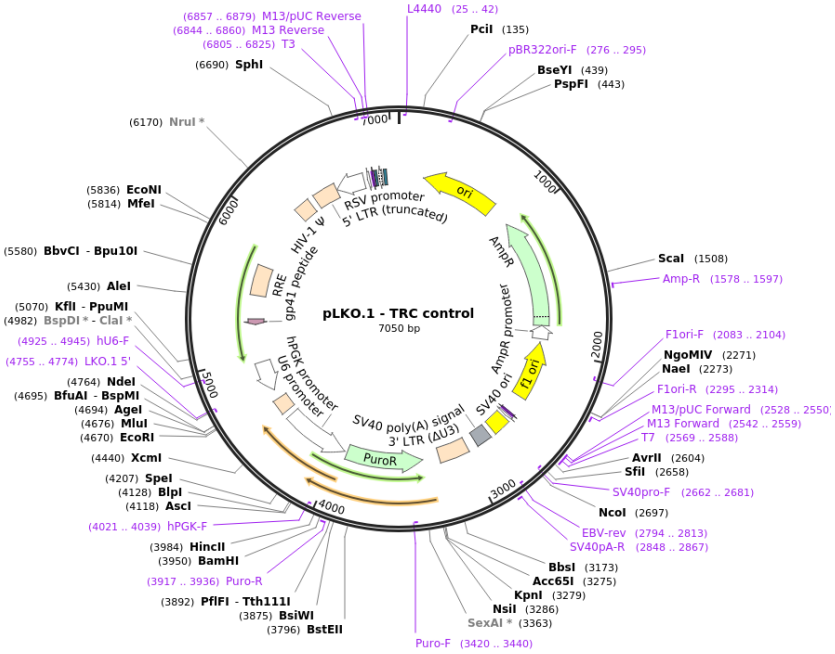

Figure 12 – Map of the pLKO.1-TRC control plasmid carrying the U6 promoter and puromycin resistance under the hPGK promoter.

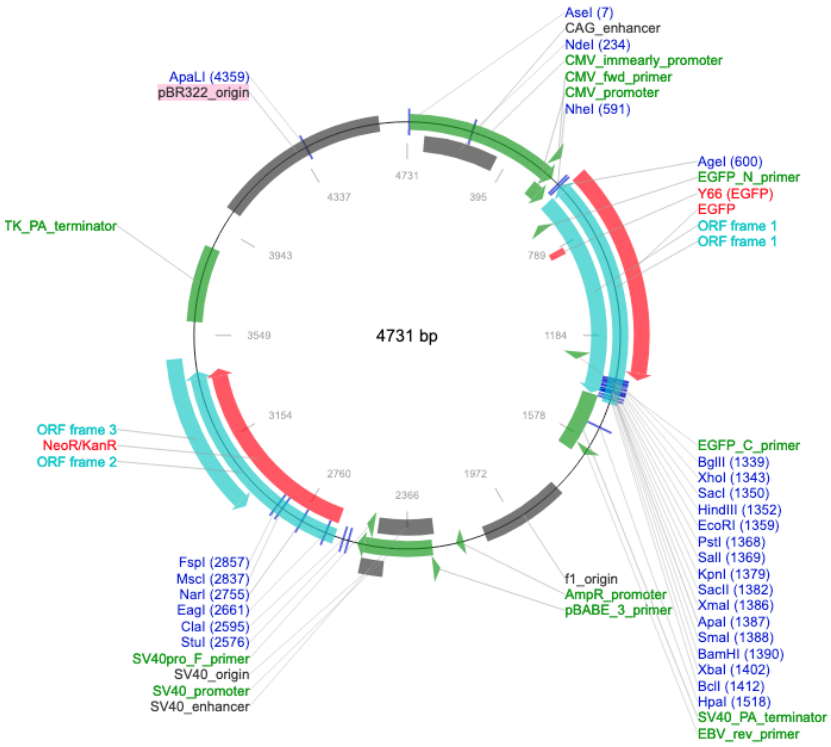

Figure 13 - Map of the pEGFP-c1 plasmid (from Clontech) expressing eGFP under the CMV promoter.

2) An experimental condition using a plasmid expressing a shRNA targeting mDia1; 5′-CGCGTGCGACGGCGGCAAACATAATTCAAGAGATTATGTTTGCCGCCGTCGCTTTTTTA -3′ (a gift from Francesca Bartollini, Columbia University; (X. Qu et al., 2017).

3) An experimental condition using a plasmid expressing a shRNA targeting mDia2: VB230213-1411qxq plasmid (pRP[shRNA]-EGFP:P2A:Puro-U6>{rat Diaph3_puro}; from Vectorbuilder) (Figure 14). This plasmid includes the sequence targeting mDIA2 (5'-CGCCCCAAGTTGCATTTAAAT-3') under the promoter U6. It also expresses EGFP:P2A:puromycin under the promoter hPGK.

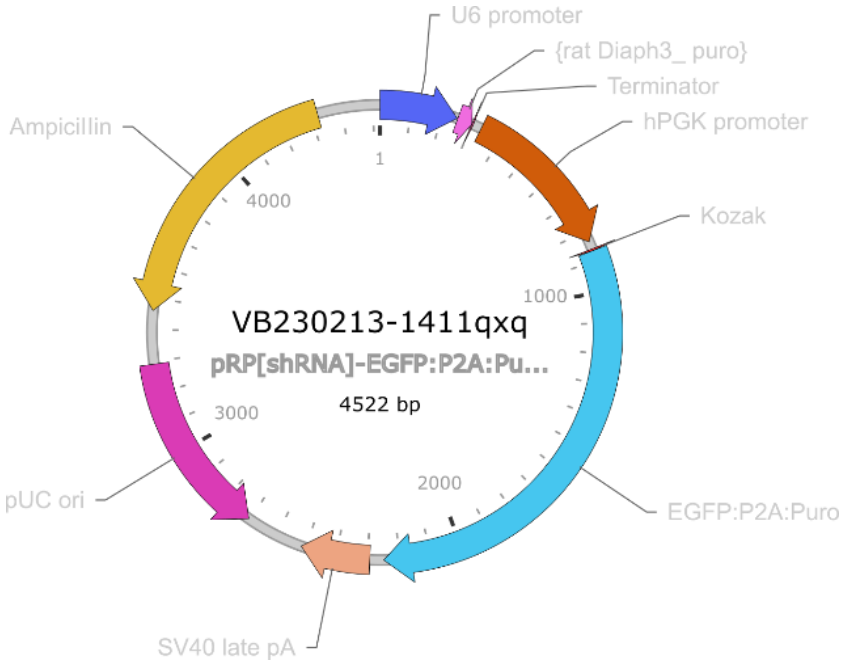

Figure 14 – Map of the VB230213-1411qxq plasmid expressing a shRNA targeting mDia2: (pRP[shRNA]-EGFP:P2A:Puro-U6>{rat Diaph3_ puro}; from Vectorbuilder). The Sh is expressed under the promoter U6 and GFP:P2A:puromycin is expressed under the promoter hPGK.

7.3 Transformation and Plasmid Production

Competent cells underwent plasmid transformation as follows: 1-2 µL (100- 200 ng) of DNA was combined with 45 µL of competent cells (NZYTech, #MB00501) in a microtube, followed by 30 minutes of ice incubation. The tubes were subsequently placed in a heating block at 42°C for 45 seconds, followed by a 2-minute ice incubation. Post-incubation, 100 µL of LB medium (NZYTech, #MB02803) was added to the bacterial suspension, and the mixture was cultured on an orbital shaker incubator at 37 °C for 1 hour. Subsequently, the transformed cells were plated onto LB plus agar plates containing ampicillin and incubated at 37°C with 5% CO_2 overnight. To initiate a starter culture of the transformed cells, an isolated colony was selected from the plate and introduced into a falcon tube containing 5 mL of LB medium (NZYTech, #MB02803) with 0.1% ampicillin (Sigma-Aldrich, #A9518-5G). The falcon was then incubated in an orbital shaker incubator ON at 37°C. The subsequent day, the starter culture was transferred to a larger erlenmeyer flask, containing 250 mL of LB medium (NZYTech, #MB02803) supplemented with 1% ampicillin (Sigma-Aldrich, #A9518-5G), and subjected to ON incubation at 37 °C in the orbital shaker incubator. Following the ON incubation, the culture was centrifuged at maximum speed for 30 minutes at 4°C. After discarding the

supernatant, the resulting pellets could be stored at 4°C for short-term use or immediately utilized. For plasmid DNA isolation, the NZYMaxiprep Kit (NZYTech, #MB05102) was employed, following the manufacturer's instructions. Briefly, the cell pellet was resuspended in 24 mL of buffer M1, containing RNase A, by vigorous vortexing. Subsequently, 24 mL of Buffer M2 (a solution of Sodium Dodecyl Sulfate) was gently added, mixed by tube inversion 5 times, and incubated at RT for 5 minutes. Buffer M1 and M2 are added in order to obtain cell lysis. This was followed by adding 24 mL of pre-cooled Buffer M3 (containing Potassium acetate), gentle tube inversion 10-15 times, and centrifugation for 30 minutes at ≥20,000 g at 4°C, allowing the neutralization of the alkaline lysis. The lysate was loaded onto an equilibrated NZYTech Plasmid Maxi Column (previously equilibrated with 6 mL buffer MEQ). A single wash of the column with 32 mL of Buffer MW was conducted, and the plasmid DNA was eluted with 15 mL of Buffer ME, recovering the liquid in a clean tube. Then, 10.5 mL of room-temperature isopropanol was added and incubated for 2 minutes at RT to precipitate the DNA. After supernatant removal, a pellet was formed by adding 5 mL of RT 70% ethanol and centrifuging at ≥15,000 xg for 10-15 minutes at RT. The ethanol was gently removed, and the pellet was air-dried at RT. Ultimately, the DNA pellet was dissolved in 100-150 µL of endotoxin-free water, and its concentration was quantified using the Nanodrop.

8. Cell Transfection

8.1 Cell Line Transfection

The day prior to the transfection, RAT-2 cells were plated in a 24-well plate at a cell density of 50,000 cells/well. Transfection was done using the Invitrogen™ Lipofectamine™ 2000 Transfection Reagent (Invitrogen™, #11668019). The media of each well was removed and 250 µL of DMEM High Glucose (Capricorn Scientific, #DMEM-HA) medium was added. Afterwards, Lipofectamine and DNA were diluted in DMEM in different eppendorfs: a) 500 ng of DNA in 50 µL of DMEM High Glucose medium per well; b) 2 µL of Lipofectamine 2000 in 50 µL of DMEM High Glucose medium per well. Mixture a) was added to mixture b) and incubated for 15 minutes at RT. To each well, 100 µL of the DNA and Lipofectamine mix was added, and cells were incubated at 37°C in a 5% CO_2 incubator for 1 hour. At the end of the incubation period, the media was removed and replaced by the cells' complete media previously heated at 37°C.

8.2 Primary Hippocampal Neuron Transfection

Hippocampal neurons underwent transfection at DIV3 and DIV8 to evaluate the effects of downregulation of Arp2/3, mDia1 and mDia2 during the formation and

maintenance of the MPS, respectively. As previously stated, on the culture day, a cell density of 50,000 cells per well was plated. Transfection was done using the Invitrogen™ Lipofectamine™ 2000 Transfection Reagent (Invitrogen™, #11668019). The media of each well was removed and 250 µL of neurobasal medium (Invitrogen, # 21103-049) was added. Afterwards, Lipofectamine and DNA were diluted in Neurobasal medium (Invitrogen, # 21103-049) in different eppendorfs: a) 500 ng of DNA in 50 µL of neurobasal medium per well; b) 2 µL of Lipofectamine 2000 in 50 µL of Neurobasal medium. Mixture a) was added to mixture b) and incubated for 15 minutes at RT. To each well, 100 µL of the DNA and Lipofectamine solution was added, and cells were incubated at 37°C in a 5% CO_2 incubator for 1 hour. At the end of the incubation period, the media was removed and replaced by the cells' complete media previously heated at 37 °C.

9. Genomic DNA Sequencing

9.1 Crude Genomic DNA Extraction

Approximately 48 hours after transfecting RAT-2 cells with using the control and experimental conditions detailed above, the plates were removed from the incubator and the media was removed from each well. Using PBS, each well was washed two times and then 250 µL of trypsin (Trypsin 0,05% EDTA (1X), Alfagene, #25300062), was added per well and incubated at 37°C in a 5% CO2 incubator for 5 minutes. After this, 250 µL of media was added to each well. Pulls of 4 wells were made and cells were centrifuged for 1000 rpms for 5 mins. Subsequent to discarding the supernatant, the cell pellet underwent a PBS wash, and another round of centrifugation was executed (1000 rpms for 5 mins), with the supernatant once again being discarded. This step was repeated. After adding 75 µL of 25 mM NaOH/ 0.2 mM EDTA, samples were heated at 98°C for 2 minutes in a heating block and then the temperature was reduced to 15°C. Finally, 75 µL of 40 mM Tris HCl (pH 5.5) was added. Samples were stored at -20°C.

9.2 Genomic DNA PCR and Analysis

Using the crude extract of genomic DNA, a PCR mix was prepared. To do so, for each sample: 6,25 µL of the Supreme NZYTaqII 2x Green Master Mix (containing Taq-derived DNA polymerases, deoxynucleotide triphosphates (dNTPs) and 2.5 mM $MgCl_2$) (NZYTech, # MB36002) was mixed with 3 µL of genomic DNA and 1 µL of primer forward and 1µL of primer reverse (Table 3). MilliQ water was added to a final volume of 12,5 µL. Then samples were placed in the thermocycler and the following program was used: a

denaturation step at 95°C for 5 min followed by 35 cycles of 94°C for 30 seconds, 60°C for 30 seconds and 72°C for 30 seconds and finally a final extension step at 72°C for 5 minutes. A 2% agarose gel was prepared using 4 g of agarose and 200 mL of 1x TAE buffer (20 mL of 50x TAE buffer (BioRad/ #161-0773) were mixed with 980 mL of water). After microwaving it for 1 to 3 minutes until the agarose was completely dissolved and cooled until about 50°C, 8 µl of the GreenSafe Premium (NZYTech/ #MB13201) was added and the liquid was poured into a casting tray with the appropriate well comb in place. The gel was let to solidify at RT for 20 to 30 minutes. At the end of the PCR, the molecular weight ladder (NZYTech/ #MB04401) and samples were loaded into the gel and placed into the gel box filled with 1xTAE (covering the gel). The gel ran for 1 hour and 30 minutes at 300 mA and 130 V. After the run, the gel was taken to the Gel Doc where the resulting bands were visualized and captured.

Table 3 – List of the used primers for the genomic DNA analysis and for cDNA analysis

Primer	**Sequence**
ARPC2 primer forward	5'-CTCAGTCCTACCCTCGCTTG-3'
ARPC2 primer reverse	5'-CCTCTCTTTCCCCCTTAGGA-3'
mDia1 primer forward	5'-TGGAGACGGAAGAAGGAATC-3'
mDia1 primer reverse	5'-CTGGCTGCGGTAGGATAC-3'
mDia2 primer forward	5'-GTGATGAGACAGGAGTGATG-3'
mDia2 primer reverse	5'-CTGAGACATTGGACTGAGAC-3'
β-actin primer forward	5'-ACCACACCTTCTACAATGAG-3
β-actin primer reverse	5'-TAGCACAGCCTGGATAGC-3'
GADPH primer forward	5'-AGGCACCAAGATACTTACAAAAAC-3'
GADPH primer reverse	5'- TGTATTGTAACCAGTCATCAGCA-3

9.3 Purification of PCR products

To purify the PCR product, the Zymoclean™ Gel DNA Recovery Kit (Zymo Research/ #D4045) was used and the manufacturer's protocol was followed. After analysing the presence of bands on the GelDoc, using UV lights the band with the correct size was identified. Using a scalpel, the correct band was excised from the gel and stored in a microtube. After that, each agarose gel slice was weighed and 300 µl of ADB buffer per 100 mg agarose gel slice was added. Next, the tubes were placed in a heating block at 55°C for a minimum of 10 minutes. When the gel slice appeared to be fully dissolved, the sample was mixed through inversion. The melted agarose solution was transferred to a Zymo-Spin™ Column in a collection tube, centrifuged for 1 minute and the flowthrough discarded. Then, 200 µL of DNA Wash Buffer was added to each column and centrifuged for 30 seconds and the flow-through was discarded. This step was repeated. Lastly, the column was placed in a microtube and 6 µL DNA Elution Buffer was added directly onto the centre of the column and subjected to a 1-minute centrifugation cycle to yield the final eluate.

9.4 Sequencing of the PCR amplicon

The DNA concentration in the PCR amplicon was determined using Qubit™ 1X dsDNA HS Assay Kit P/N Q33231 was used. After that, DNA Sequencing was performed by the i3s' Genomic Platform employing the Sanger Sequencing Reaction method using the Applied Biosystems 3500 Genetic Analyzer (S/N 29113-030). The results were analysed using SnapGene Software.

10. RNA and cDNA Extraction and PCR

10.1 RNA Extraction

For RNA Extraction the NZY Total RNA Isolation kit (NZYTech, #MB13402) was used and the manufacturer's instructions were followed. Upon removal of the transfected cells from the incubator, the 24-well plate was placed on ice and, after discarding the cell media, 350 µL of buffer NR and 3.5 µL β-mercaptoethanol were added to each pull of 4 wells. The resulting lysate was then transferred into a NZYSpin Homogenization column placed in a 2 mL collection tube. After centrifugation at 11,000 xg for 1 minute, the resultant flow-through was transferred to a fresh 1.5 mL microcentrifuge tube, to which 350 µL of 70% ethanol was introduced and mixed immediately by pipetting up and down. The lysate was loaded into a NZY Spin Binding column and centrifuged at 11,000 g for 30 seconds. After discarding the flowthrough, a total of 95 µL of the Digestion Mix

(comprising 10 µL of DNase I and 90 µL of Digestion buffer) was meticulously added. The mixture was allowed to incubate at room temperature 15 minutes. Subsequent to the incubation, 200 µL of Buffer NWR1 was added to each sample, followed by centrifugation at 11,000 g for 1 minute. The addition of 600 µL of Buffer NWR2 followed by centrifugation at 11,000 g for 1 minute was repeated twice. Finally, each column was carefully placed within a clean Microtube. A total of 40 µL of RNase-free water was introduced into each column. Following a last centrifugation at 11,000 g for 1 minute, RNA was stored at -20°C for short-term utilization.

10.2 cDNA Extraction

For cDNA Extraction, the NZY First-Strand cDNA Synthesis Kit (NZYTech, #MB12502) was used. On ice, the following reaction components were added into a sterile nuclease-free microcentrifuge tube: 10 µL NZYRT 2× Master Mix, 2 µL NZYRT Enzyme Mix, 1 to 3 ug of RNA and DEPC-treated H_2O to achieve a final volume of 20 µL. After gently mixing the components, the tubes were placed in the thermocycler following the program: 25°C for 10 minutes, 50°C for 30 minutes and 85°C for 5 minutes. The samples were chilled in ice and after adding 1 µL of NZY RNase H, were incubated at 37°C for 20 min.

10.3 PCR

For each cDNA sample, the following PCR Mix was prepared: 6,25 µl of the Supreme NZYTaqII 2x Green Master Mix was mixed with 1 µl of cDNA, 1 µl of primer reverse and 1µl of primer reverse (Table 3). MilliQ water was added to a final volume of 12,5 µl. Then the samples were placed in the thermocycler and the following program was used: a denaturation step at 95 °C for 5 min followed by 35 cycles of 94 °C for 30 seconds, 60 °C for 30 seconds and 72 °C for 30 seconds and finally a final extension step at 72 °C for 5 minutes. PCR products were analysed following electrophoresis as detailed above in Genomic DNA PCR and Analysis.

11. STED Imaging

STED imaging was performed on an inverted Leica Stellaris STED 3 using DIV5 and DIV14 hippocampal neurons. Hippocampal neurons were imaged at the AIS and the shaft, approximately at a distance of 80-100 µm from the cell body, with a HC PLAPO 93x NA 1.4 STED glycerol objective (Leica Microsystems) using confocal and STED

modes. The 2D vortex STED images with lateral resolution enhancement were recorded with 20 nm pixel size in xy and dwell times of typically 600 ns. First, the STED far-red channel (Abberior STAR 635P) was recorded with 633 nm excitation using the pulsed white light laser with 80 MHz repetition rate and STED depletion was performed with a synchronised pulsed 775 nm depletion laser. The detection bandpass was set to 650 to 750 nm and the pinhole was set to 0.93AU. The following acquisition settings were applied: 16 x line averaging and detector gating on a Hybrid Detector (HyD, Leica Microsystems) of 0.3 ns to 6 ns. The second STED channel (Abberior STAR580) was recorded in line sequential mode with 561 nm excitation and 775 nm depletion using a detection window from 580 to 620 nm. All other settings remained constant. To analyse the % of MPS abundance, we measured the length of the axon and determined the % of length including positive actin rings.

12. Statistical Analysis

The data is presented as the mean ± standard error of the mean (SEM). Statistical analysis was performed by GraphPad Prism, version 6.01 for Windows (GraphPad Software, California, USA). For most experiments, the statistical significance was evaluated using the Student's t-test. The effect of drugs on MPS within the AIS and Shaft was evaluated by two-way ANOVA followed by Fisher’s pos hoc LSD test. Statistical significance was determined by a p-value less than 0.05.

Results

1. Inhibition of Arp2/3 activity compromises the formation and maintenance of the MPS

1.1 CK869 does not affect cell morphology

As previously indicated, it is our main aim to investigate how actin nucleates and elongates within the rings of the MPS. Thus, the role of the Arp2/3 protein in this process is being evaluated. Arp2/3 is an ABP involved in the polymerization of branched actin filaments. We intended to inhibit the polymerization ability of this protein by using a chemical drug, CK869 (Hetrick et al., 2013). Hence, it was imperative to assess its effects on cell morphology, axon and dendrite length, in order to confirm that the observed outcomes were indeed a consequence of diminished Arp2/3 activity, as opposed to cell unviability. To achieve this, hippocampal neuron cultures were acutely treated with CK869 for one hour, and neurite outgrowth was quantified upon immunostaining against βIII tubulin, a neuronal specific protein. As the results demonstrate, CK869, at this concentration (10uM), does not affect dendrite or axon length compared with the control conditions, as showed in Figure 15A and the respective quantifications (Figure 15B) thus validating our experimental approach (Figure 15).

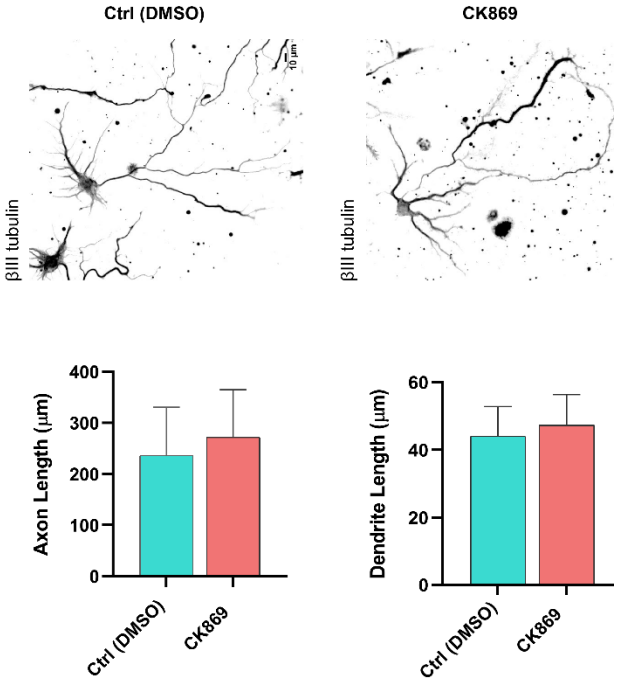

Figure 15- CK869 (10 µM) does not affect dendrite or axon length. A) Representative images of embryonic hippocampal neuron cultures at DIV5 stained with βIII tubulin, upon treatment with DMSO (Ctrl, left image) or 10 µM CK869 (right image) for one hour before fixation. **B)** Respective quantifications of the axon (left) and dendrite length (right) measured using the plugin NeuronJ (Fiji). Scale bar: 10 µm. Data represent mean ± SEM (ns – nonsignificant, two-tailed paired t-test) ; n= 25 neurons.

1.2 CK869 affects the abundance of MPS in neurons

To study the role of Arp2/3 in the formation and maintenance of MPS, we acutely incubated primary hippocampal neurons with CK869 (10 µM) at DIV5 and DIV14, respectively. The MPS is only detected using nanoscopy techniques. Treated neurons were immunostained for 2 phospho myosin light chain (2xphospho MCL), a specific marker of the AIS, and for actin (phalloidin) and visualized in a tau-STED microscope. As depicted in Figure 16 our results show that in both the time points analysed, DIV 5 (formation) and DIV14 (maintenance), both the axonal compartments, AIS and shaft, present a reduction in the percentage of the MPS' abundance to approximately 50% of the initial values. In contrast, control neurons, treated with DMSO, did not show any disturbance in the organization of the MPS. These results support that Arp2/3 is involved both in the formation and maintenance of the actin rings within the MPS.

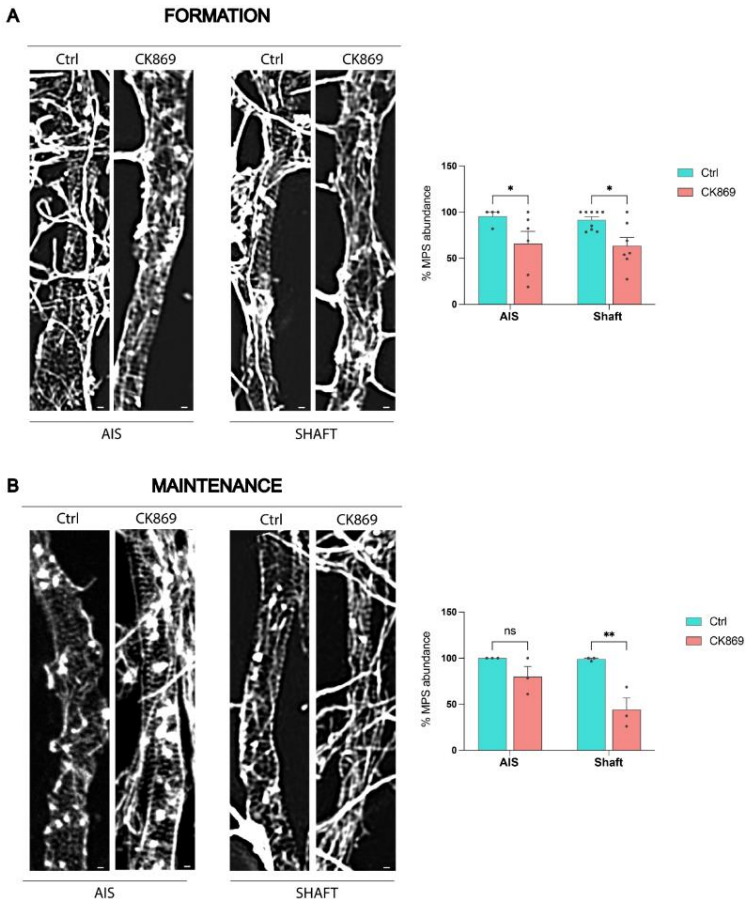

Figure 16 - CK869 decreases the abundance of organized MPS in the AIS and shaft of the neurons. A) Tau-STED images of embryonic hippocampal neuron cultures at DIV5, either control or treated with CK869 (10 µM) stained with phalloidin. The respective quantification is shown in the graph at the right. Data represent mean ± SEM (ns – nonsignificant**,** two-way ANOVA followed by Fisher's pos hoc LSD test); n= 6-8 neurons. **B)** Tau-STED images of embryonic hippocampal neuron cultures at DIV14 either control or treated with CK869 (10 µM) stained with phalloidin. Scale bar: 0.2 µm. The respective quantification is shown in the graph at the right. This data represent mean ± SEM (ns – nonsignificant, p-value ** < 0.01, two-way ANOVA followed by Fisher's pos hoc LSD test) of 3 independent experiments, where 6-8 neurons were quantified in each experiment for each condition.

1.3 Genetic Manipulation using CRISPR-Cas9 is efficient in abolishing ARPC2 expression

To confirm our results obtained with chemical inhibition of Arp2/3, we developed a genetic approach based on CRISPR-Cas9 system to target exon2 of the ARPC2 gene. Simultaneously, targeting of the ROSA26 locus was used as a control. The efficiency of this method was assessed through various molecular assays, such as analyses of the genomic DNA and mRNA levels in RAT-2 cells (a rat fibroblast cell line) and immunofluorescence in hippocampal neurons.

1.3.1 Validation using Genomic DNA

To further validate the efficacy of the CRISPR-Cas9 system using guide RNA targeting the ARPC2 subunit, we performed genomic DNA sequencing on transfected RAT-2 cells. Our initial hypothesis for this approach was to insert indels (insertions or deletions of nucleotides) within exon2, that would impact the expression of ARPC2. Two sets of neurons were prepared: one was transfected with the guide RNA targeting the ARPC2 subunit and another set transfected with a guide RNA targeting the ROSA26 locus and used as a control. Genomic DNA was extracted from both sets for Sanger sequencing. Control neurons revealed a perfect alignment with the wild-type (WT) sequence (Figure 17A). In contrast, when analysing the sequencing results for the ARPC2 mutant cells, distinct additional peaks were observed in the electropherogram (Figure 17B). These additional peaks corresponded to the presence of indel regions, thus showing that the CRISPR-Cas9 was effective. Due to the high percentage of non-transfected neurons, the specific mutations produced remain inconclusive.

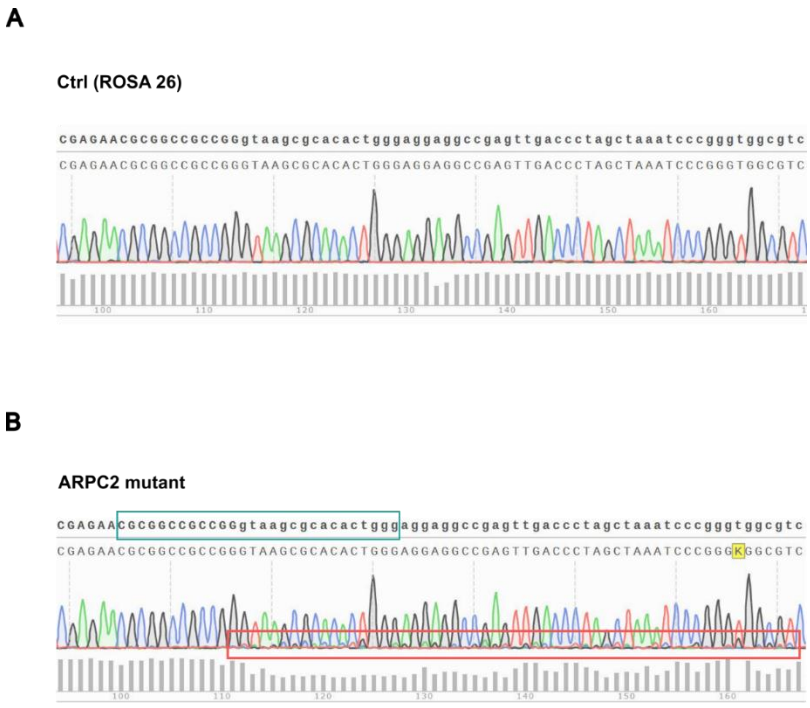

Figure 17 - Validation of the CRISPR-Cas9 genetic manipulation through Genomic DNA sequencing indicates that the technique proves to be effective. A) Image acquired using the SnapGene Software where the sequence obtained from the sequencing of the genomic DNA of the control cells transfected with CRISPR-Cas9 targeting the Rosa26 was aligned with the WT sequence of ARPC2. **B)** Image acquired using the SnapGene Software where the sequence obtained from the sequencing of the genomic DNA of the cells transfected with CRISPR-Cas9 targeting the ARPC2 was aligned with the WT sequence of ARPC2.

1.3.2 Validation of ARPC2 CRISPR-Cas9 using cDNA

In addition to our previous experiments, we conducted analyses of the mRNA levels to complement our findings. Following the same experimental setup for cell transfections, we extracted cDNA from a population of RAT-2 cells transfected with a guide RNA targeting ARPC2 and a control population transfected with a guide RNA targeting ROSA26. Subsequently, we performed PCR on the cDNA samples and quantified the resulting bands. Unfortunately, our analysis did not reveal any significant differences between the cDNA of the control and ARPC2 neurons (Figure 18). This outcome was not entirely unexpected, given the limitations we encountered earlier. As mentioned, our sample did not consist of a high proportion of transfected cells. To address these challenges, ongoing efforts are focused on enhancing the selection with the appropriate antibiotic (puromycin) of transfected cells in order to achieve a higher representation of transfected cells within our samples. This strategy aims to provide a more accurate and meaningful assessment of cDNA differences between the control and ARPC2 groups.

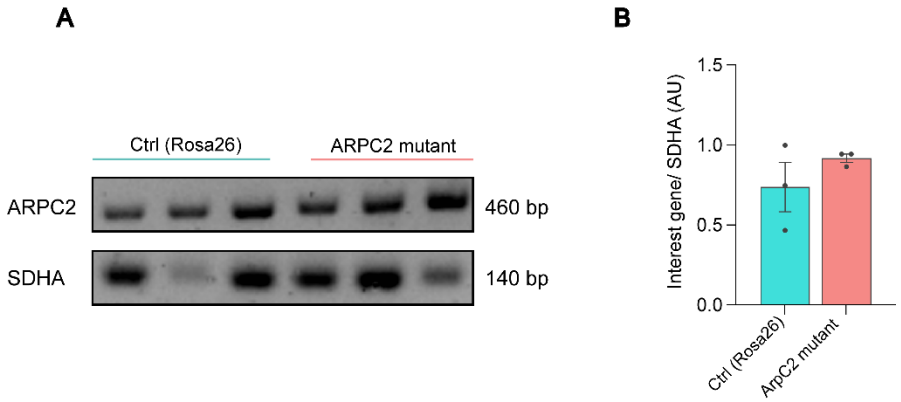

Figure 18 - Validation of the CRISPR-Cas9 genetic manipulation through cDNA analysis showed no differences in cDNA levels. A) Images of the PCR acquired in the GelDoc and **B)** Quantitive analysis of the gene of interest (ARPC2) normalized by the constitutive gene SDHA for control neurons and neurons where ARPC2 CRISPR-Cas9 was done. Data represent mean ± SEM (ns – nonsignificant, two-tailed paired t-test); n=3.

1.3.3 Validation of ARPC2 CRISPR-Cas9 using Immunofluorescence

Hippocampal neurons were transfected with plasmids containing the CRISPR-Cas9 system and a guide RNA specific to exon2 of the ARPC2 subunit aiming prevent the formation of the Arp2/3 complex. To validate the success of this genetic approach, immunofluorescence assays were conducted on the transfected hippocampal neurons. Upon immunostaining against one of the Arp2/3 subunits, ARPC5 or p16, and visualization in a widefield microscope, the levels of this protein were quantified in both transfected and non-transfected cells for both conditions, control and ARPC2 mutant neurons. As depicted in Figure 19, the cells in which ARPC2 expression was suppressed exhibited a significant reduction in the levels of ARPC5 subunit when compared to the non-transfected neurons. This suggests that the CRISPR-Cas9 targeting ARPC2 is effective, resulting in a significant reduction in Arp2/3 expression within the neurons.

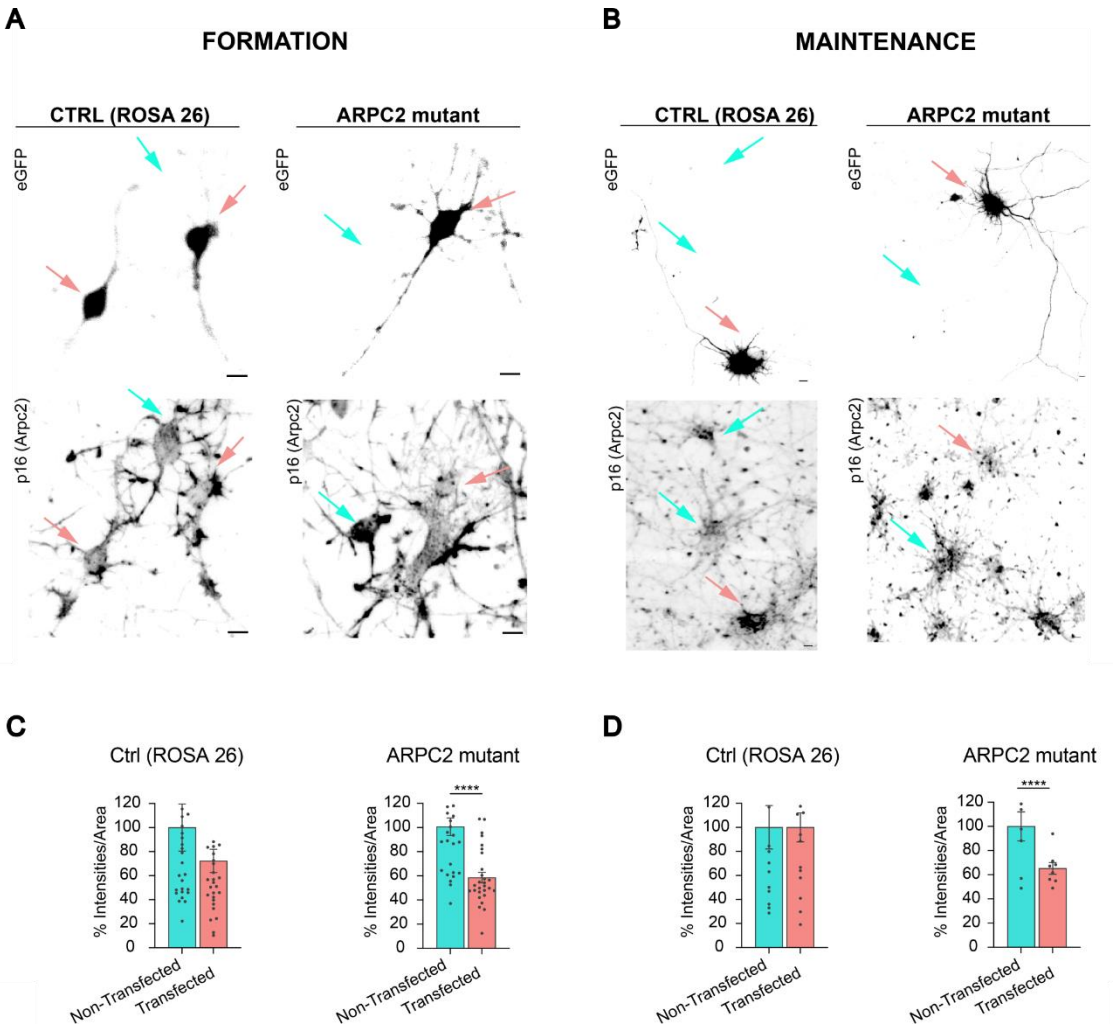

Figure 19 - Validation of the ARPC2 CRISPR-Cas9 through Immunofluorescence. Representative images of embryonic hippocampal neuron cultures transfected with ROSA26 or ARPC2 and Cas9 and stained for ARPC5 (p16) at DIV5 (**A**) and DIV14 (**B**); ARPC2 mutant cells (in magenta) are eGFP positive, and control neurons (in blue) are eGFP negative. Scale bar 10 μM. **C)** Quantitative analysis of the intensity of p16 normalized by area at DIV5. **D)** Quantitative analysis of the intensity of p16 normalized by the area at DIV14. Data represent mean ± SEM (ns – nonsignificant, p-value **** < 0.0001, two-tailed paired t-test); 25 neurons per experimental condition.

1.4 Arp2/3 is important for the formation and maintenance of an organized MPS

To assess the impact of Arp2/3 absence in the MPS and the actin rings, hippocampal neuron cultures were transfected with the respective constructs, and upon fixation, at time points at which formation (DIV3-DIV6) or and maintenance (DIV10-DIV14) of the MPS takes place, neurons were immunostained for 2xphopho MLC (AIS marker) and for actin (phalloidin). Neurons were then visualized in a Tau-STED microscope. For both the time points analysed (formation and maintenance), ARPC2 mutant neurons presented a disruption in the actin rings within the MPS, that was not observed for the neurons transfected with ROSA26 (Figure 20 and Figure 21). Moreover, non-transfected neurons

for both conditions showed an organized MPS. This demonstrates that neurons with reduced levels of Arp2/3 do not have an organized MPS, while control ones (eGFP-negative) present an organized MPS. Importantly, these results indicate the importance of Arp2/3 complex for the adequate formation and maintenance of the MPS.

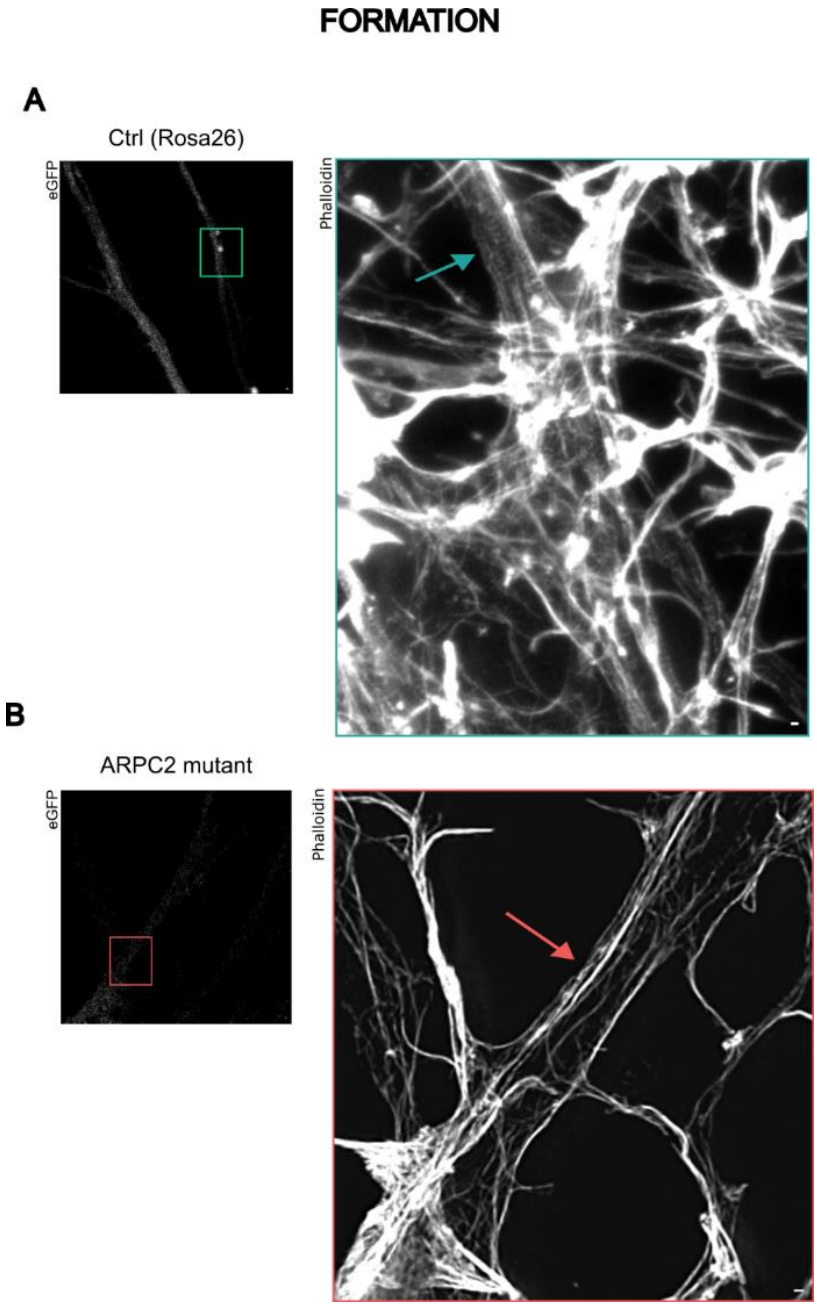

Figure 20 - Arp2/3 is important for the formation of the MPS. A) Representative images from embryonic hippocampal neuron cultures at DIV5, of a control cell transfected with the CRISPR-Cas9 plasmid and the guide targeting ROSA26 locus stained with phalloidin. On the upper left panel, a confocal image of a control neuron expressing eGFP is shown. The respective inlet, corresponding to the tau-STED image, shows a complete organized MPS (blue arrow). **B)** Representative images from embryonic hippocampal neuron cultures at DIV5, of a ARPC2 neuron transfected with the CRISPR-Cas9 plasmid and the guide targeting ARPC2 (eGFP positive cell) stained with phalloidin. On the bottom left panel, a confocal image of a ARPC2 mutant cell expressing eGFP is shown. The respective inlet, corresponding to the tau-STED image, shows a MPS completely disrupted and lacking actin rings (pointed by the magenta arrow). Scale bar: 0.2 µm.

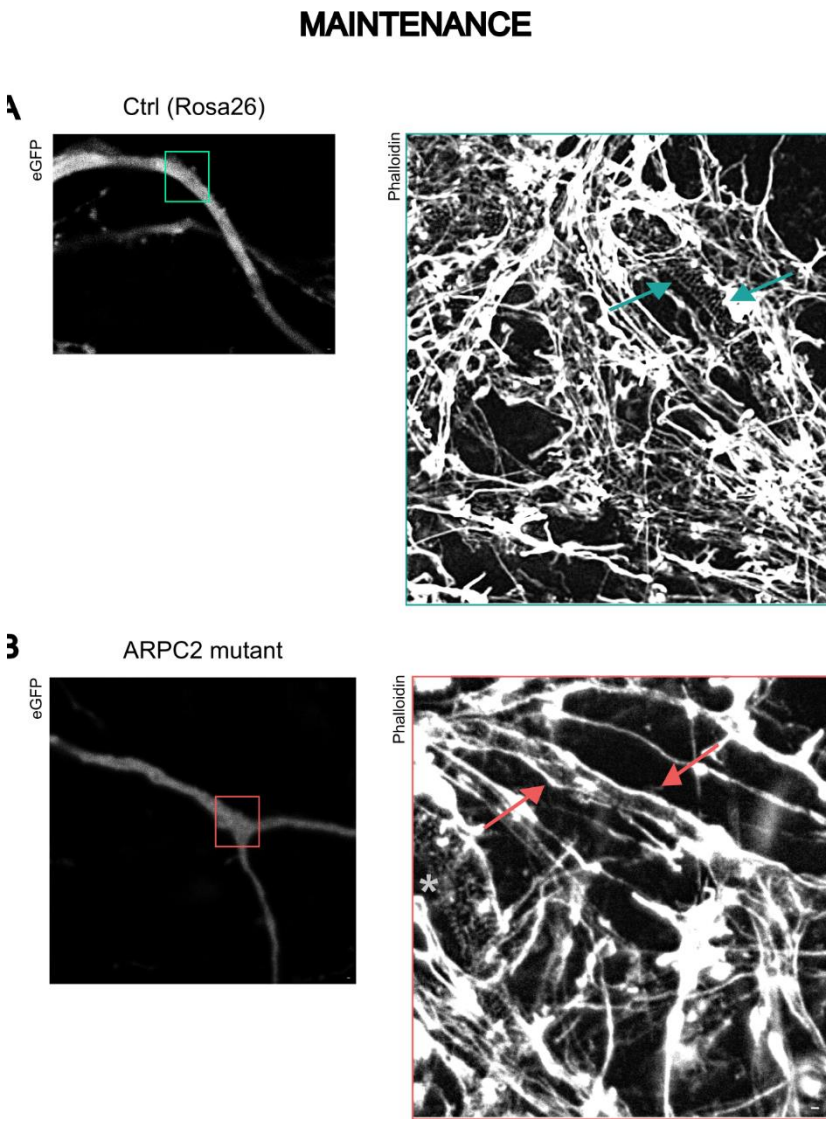

Figure 21 - Arp2/3 is important for the maintenance of the MPS. A) Representative images from embryonic hippocampal neuron cultures at DIV14, of a control neuron transfected with the CRISPR-Cas9 plasmid and the guide targeting ROSA26 locus stained with phalloidin. On the upper left panel, a confocal image of a control ROSA26 neuron expressing eGFP is shown. The respective inlet, corresponding to the tau-STED image, shows a complete organized MPS (magenta arrow). **B)** Representative images from embryonic hippocampal neuron cultures at DIV14 of a ARPC2 mutant cell transfected with the CRISPR-Cas9 plasmid and the guide targeting ARPC2 (eGFP positive cell) stained with phalloidin. On the bottom left panel, a confocal image of a ARPC2 mutant cell expressing eGFP is shown. The respective inlet, corresponding to the tau-STED image, shows a MPS completely disrupted and lacking actin rings (pointed by the magenta arrow). A non-transfected process presents an organized MPS (grey asterisk).

1.5 The ARPC5 subunit of Arp2/3 complex has higher endogenous levels at early DIVs

Upon STED microscopy, we realized that there was a disparity in the intensity of Arp2/3 staining (using anti-ARPC5 or p16) when comparing early DIVs (DIV5) and later DIVs (DIV14), as evidenced in Figure 22A. To gain a deeper understanding on the different levels of the protein at different neuronal developmental stages, we conducted

quantifications using specific plugins from Fiji of ARPC5 (p16) intensity at both DIV5 and DIV14, as illustrated in Figure 22B. Our results unequivocally demonstrate a a notably higher abundance in ARPC5 (or p16) levels as at early time points of neuronal development (DIV5) when compared to later timepoints (DIV14). In summary, we demonstrate that Arp2/3 is fundamental for the formation and maintenance of the actin rings within the MPS.

In summary, we demonstrate that Arp2/3 is fundamental for the formation and maintenance of the actin rings within the MPS.

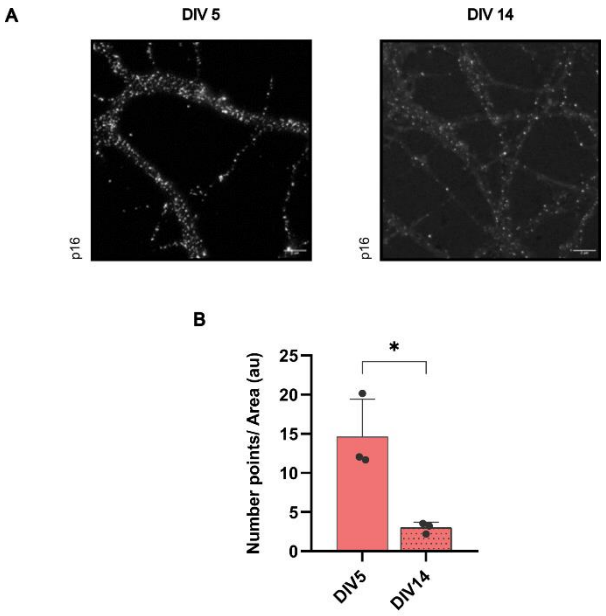

Figure 22 – The ARPC5 subunit of Arp2/3 complex has a higher endogenous expression at early neuronal developmental stages. A) Representative images of embryonic hippocampal neuron cultures at DIV5 and DIV14 stained with anti-p16 (ARPC5) antibody acquired in the STED microscope. **B**) Quantification of the endogenous expression of p16 (ARPC5) normalized by the area. Scale bar: 1 µm. Data represent mean ± SEM (p-value * < 0.05, two-tailed paired t-test) of 3 independent experiments, where 6-10 neurons were quantified in each experimental condition.

2. Reducing the expression of formins affects the formation of the MPS

2.1 Acute treatment with SMIFH2 does not affect neuronal morphology

Similarly to CK869, the effect of SMIFH2, a general inhibitor for formins (Rizvi et al., 2009) on cell morphology was also assessed to discard the possibility of cell toxicity. To do so, hippocampal neuron cultures were acutely treated with SMIFH2 (25 µM) for 25 minutes and neurite outgrowth was quantified, upon immunostaining the neurons for βIII tubulin, a neuronal-specific protein. As shown in Figure 23, at this concentration of SMIFH2 there is no difference in dendrite and axon length when compared to the control untreated neurons, thus validating this set of conditions as optimal.

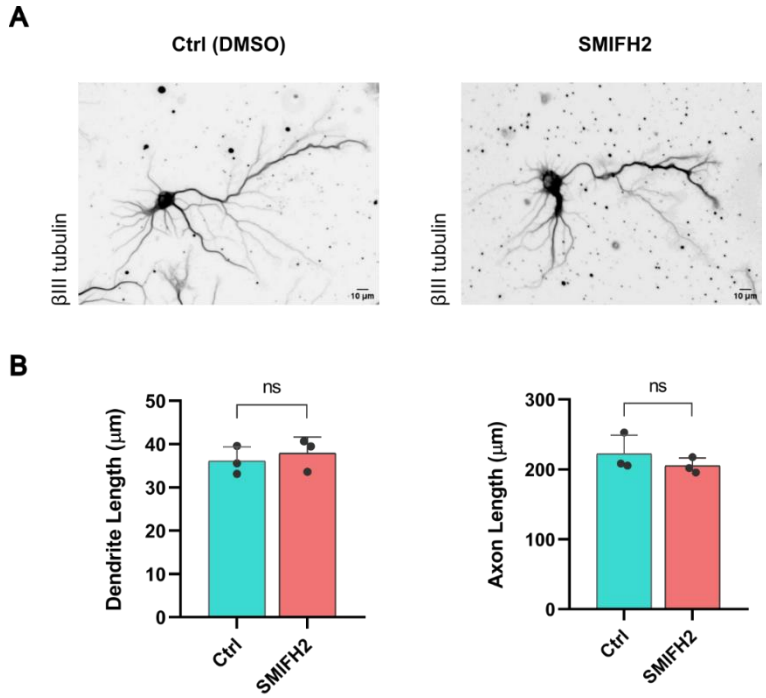

Figure 23 – Treatment with SMIFH2 (25µM, acute) does not affect dendrite or axon length. A) Representative images of embryonic hippocampal neuron cultures at DIV5 stained with βIII tubulin, upon treatment with DMSO (Ctrl, left image) or 25 µM SMIFH2 (right image) for 30 minutes before fixation. **B)** Respective quantifications of the axon and dendrite length measured using the plugin Neuron J (Fiji). Data represent mean ± SEM (ns – nonsignificant, two-tailed paired t-test) of 3 independent experiments, where 50 neurons were quantified in each experimental condition.

2.2 SMIFH2 affects MPS formation

To visualize the actin rings and elucidate if and when formins influence these structures, we used STED microscopy, on neurons immunostaining for 2xphospho MLC and actin (Figure 24). At the early time point analysed (DIV5), in contrast to the control, neurons treated with SMIFH2 show a MPS compromised in both axonal compartments

analysed, AIS and shaft. This strongly suggests that at early DIVs, formins, play a pivotal role in the formation of MPS within the AIS and shaft regions of the axon.

When extending our research to later timepoints (DIV14), the obtained results presenting a noteworthy contrast to the previous ones. Both control and treated cells exhibited an organized MPS in both the AIS and the shaft at DIV14 (Figure 24A) as demonstrated in Figure 24A. These findings suggest that formins are not essential for the maintenance of the MPS.

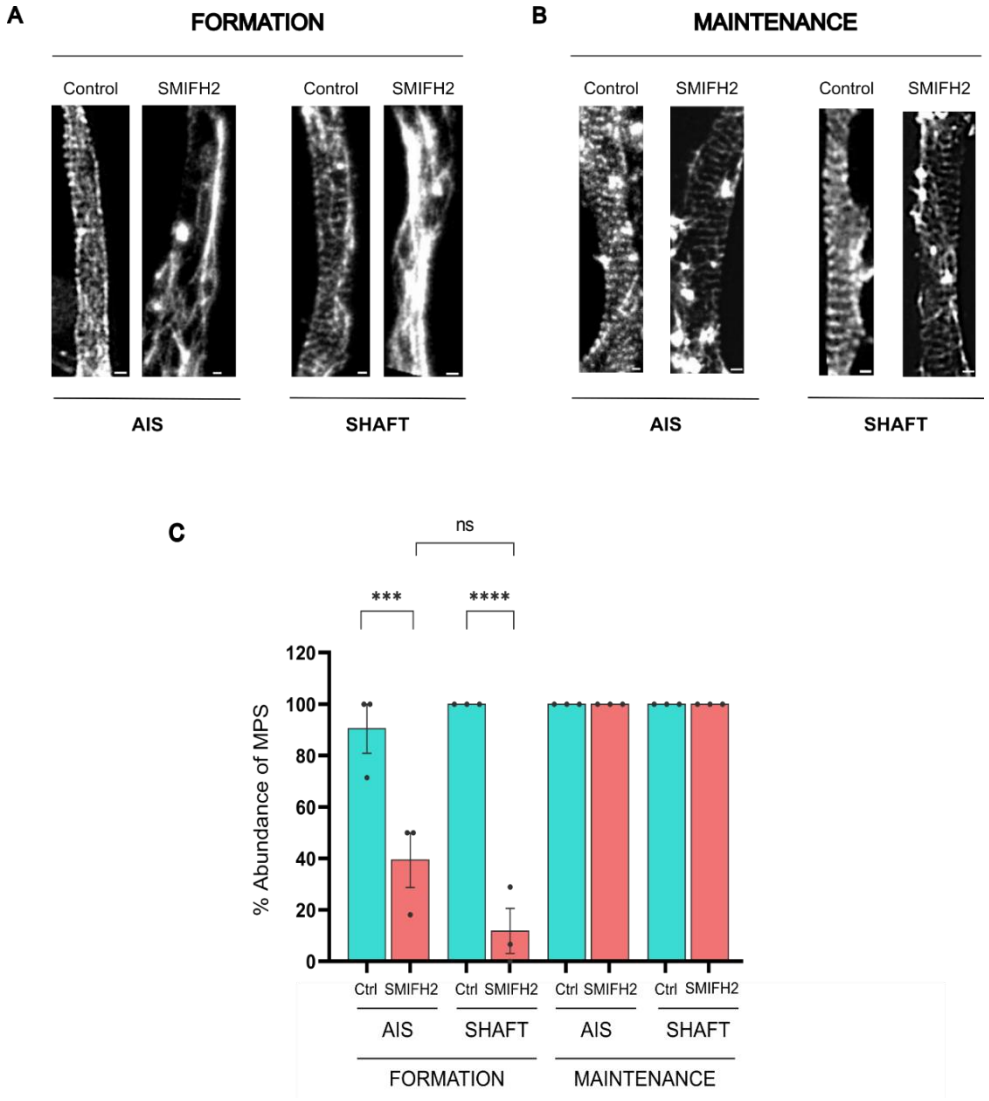

Figure 24- SMIFH2 decreases the abundance of organized MPS in the AIS and shaft of neurons during its formation. Tau-STED images of embryonic hippocampal neuron cultures at DIV5 (**A)**) and at DIV14 (**B)**) acutely treated with SMIFH2 (25 µM) stained with phalloidin. Scale bar: 0.2 µm. **C**) The respective quantification is shown in the graph. This data represent mean ± SEM (ns – nonsignificant**,** p-value ******* <0.001 two-way ANOVA followed by Fisher's pos hoc LSD test) of 3 independent experiments, where 6-8 neurons were quantified in each experimental condition.

2.3 Genetic Manipulation using shRNA appears to be efficient in reducing mDia1 and mDia2 expression

To validate our findings from the chemical inhibition of formins, we implemented a genetic approach employing shRNA to target the expression of mDia1 and mDia2. As a control, we used a pLKO plasmid containing eGFP. The effectiveness of this method was evaluated through the analysis of mRNA levels in RAT-2 cells (a rat fibroblast cell line) and immunofluorescence assays in hippocampal neurons.

2.3.1 Validation using cDNA

To further validate the chosen genetic approach for both mDia1 and mDia2, cDNA was extracted for qPCR analysis of the targeted mRNAs. Upon analysing the results, a reduction in the intensity levels of mDia1 was observed (Figure 25A). However, for mDia2, we did not detect any substantial alteration in its cDNA levels (Figure 25B). It's worth noting that, similar to our earlier ARPC2 validation experiments, our sample did not consist of an ideal proportion of transfected cells. As a result, the extracted cDNA also included non-transfected cells. To overcome these constraints and attain more conclusive findings, we acknowledge the necessity for further experiments in which a selection with proper antibiotic will be performed.

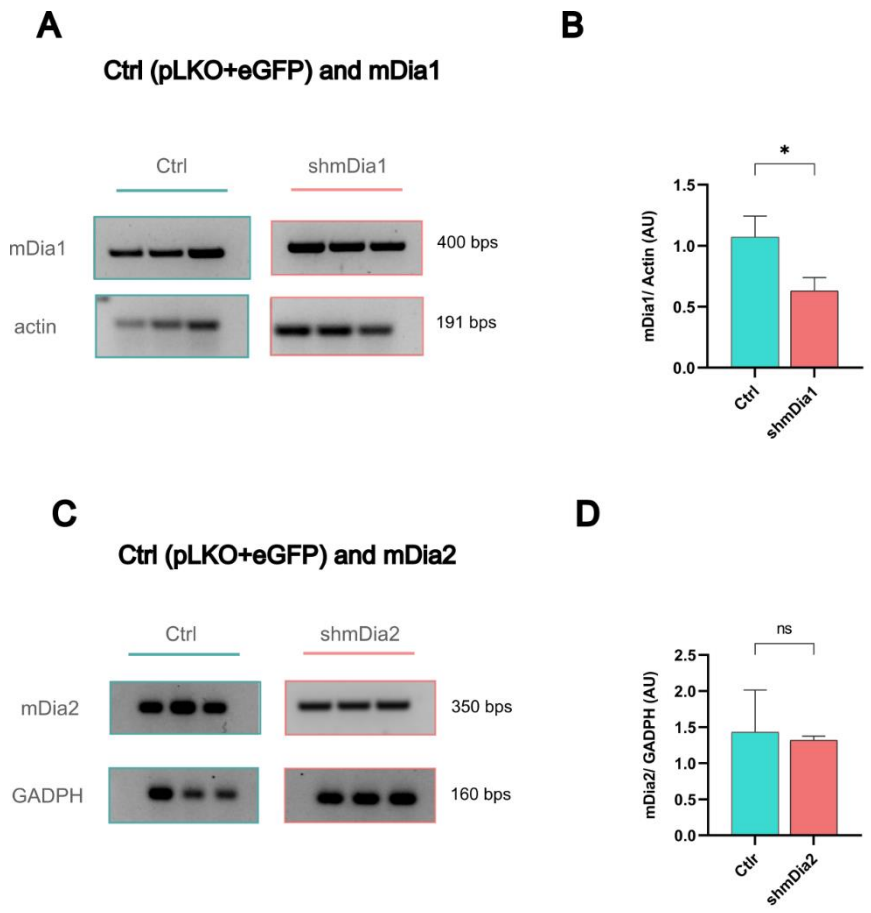

Figure 25 – Analyses of shRNA mediated downregulation of the mDia1 and mDia2. RT-PCR following shRNA-mediated knockdown of mDia1 (**A)**; upper panel) and mDia2 (**C)**; bottom panel) after transfection of RAT-2 cells. Cells were co-transfected with empty pLKO.1 vector and eGFP (Ctrl) or with plasmids encoding specific shRNAs for mDia1 or mDia2. β-actin (upper panel) and GAPDH (bottom panel) were used as housekeeping genes. Triplicates are shown. **B)** and **D)** Quantifications related to A) and B), respectively. The data represent mean ± SEM (ns – nonsignificant, p-value * < 0.05, two-tailed paired t-test); n=3**.**

2.3.2 Validation using Immunofluorescence

As mentioned in the Introduction, mDia 1 and mDia 2 belong to the formin family of proteins and are important in neuronal biology (Higgs, 2005). To evaluate whether these specific formins are involved in MPS formation, specific shRNAs were used. The primary objective was to diminish the expression levels of mDias within transfected neurons. To validate the effectiveness of this approach, immunofluorescence assays were performed. Following image acquisition using a widefield microscope, the levels of mDia1 and mDia2 were quantified in both transfected (T) and non-transfected (NT) neurons. The neurons in which mDia1 (Figure 26) and mDia2 (Figure 26) expression was downregulated exhibited a significant reduction in mDia1 and mDia2 intensity when compared to the control cells. This shows that both the shRNAs are working as expected, resulting in a decrease in mDia1 and mDia2 expression.

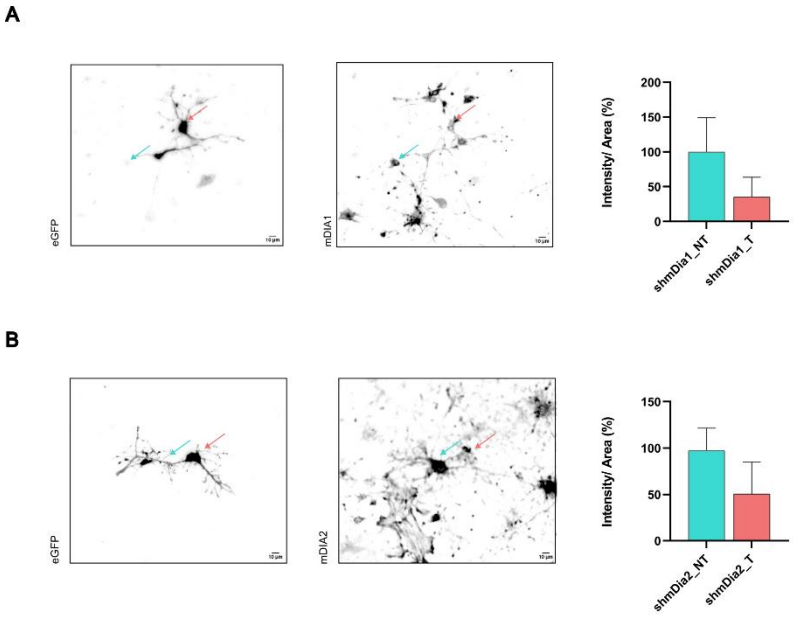

Figure 26- Validation of the shRNA targeting mDia1 and mDia2 through immunofluorescence indicates that the technique is effective in both conditions. A) On the left, representative images of embryonic hippocampal neuron cultures at formation (DIV5) stained for mDia1 and expressing eGFP (transfected cells only). shmDia1 neurons (magenta arrow) are eGFP positive, and control cells (blue arrow) are eGFP negative. On the right quantitative analysis of the intensity of mDia1 normalized by the area of non-transfected cells and transfected cells. **B)** On the left, representative images of embryonic hippocampal neuron cultures at formation (DIV5) stained for mDia2 and expressing eGFP (transfected cells only). shmDia2 neurons (magenta arrow) are eGFP positive, and control cells (blue arrow) are eGFP negative. On the right quantitative analysis of the intensity of mDia2 normalized by the area of non-transfected cells and transfected cells. This preliminary data represent mean ± SEM (p-value **<0.01, p-value **** < 0.0001, two-tailed paired t-test); n=25 neurons quantified per experimental condition.

2.4 mDia1 and mDia2 are important for the formation of the MPS

We next evaluated the effect of a reduced expression of mDia1 and mDia2 in actin ring distribution within the MPS at DIV 5, since SMIFH2 is only able to disturb the MPS at early time points. STED analysis suggests that both formins mDia1 and mDia2 affect the formation of the actin rings within the MPS (Figure 27). Control neurons transfected with an empty vector show an organized MPS structure throughout the axon whereas neurons with decreased levels of either mDia1 or mDia2 fail to form an organized MPS. These results indicate that several formins participate in the formation of the MPS.

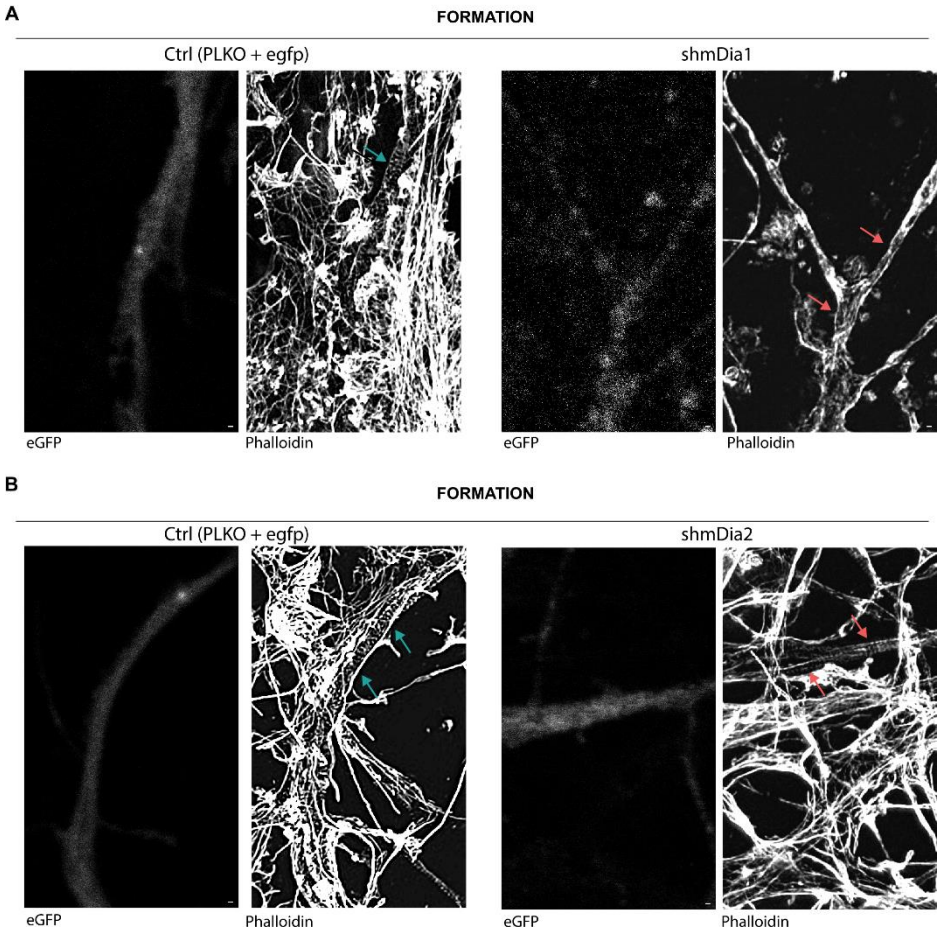

Figure 27- Formins are important for the formation of the MPS. A) On the upper panel, tau-STED images from hippocampal control neurons co-transfected with a pLKO plasmid combined with an eGFP plasmid (eGFP positive cell) and neurons transfected with shRNA targeting mDia1 stained with phalloidin. **B)** On the bottom panel, tau-STED images from hippocampal control neurons co-transfected with a pLKO plasmid combined with an eGFP plasmid (eGFP positive cell) and neurons transfected with shRNA targeting mDia2 stained with phalloidin. Scale bar: 0.2 µm.

Discussion

The MPS is one of the most intricate and complex structures within neuronal cells. Comprising an arrangement of actin rings periodically spaced by spectrin tetramers throughout the axon, this structure not only supports the thin axons, as initially described, but also acts as a platform for signalling processes, controls AIS filtering mechanism, and regulates axonal diameter (Costa & Sousa, 2021). Previous findings from our laboratory showed that when α-adducin is knocked out from neuronal cells, the MPS still presents actin rings, however with a significant increase in their diameter, thus suggesting that α-adducin is involved in the maintenance of axonal diameter (Leite et al., 2016b). Moreover, non-muscle myosin II (NMII) an ABP known to be involved in actin contraction and relaxation events, was also found to be able to regulate axonal diameter, with critical implications for the velocity of signal propagation (Costa et al, 2020) and transport of large cellular cargoes within neurons (Menier et al., 2020). We also examined the structure of NMII in hippocampal neurons and found that it exists as contracting 300 nm-bipolar filaments (Costa et al., 2020). While the importance of the MPS for the neuron is widely recognized, the precise mechanisms governing its structure, formation, and maintenance remain elusive. To address some of these concerns, this thesis focused on investigating the participation of two actin-binding nucleators, Arp2/3 and formins, in the formation (DIV5) and maintenance (DIV14) of the actin rings within the MPS.

The Arp2/3 complex is a seven-subunit protein complex crucial to branched actin filament formation in neuronal cells. In 2013, a study described two drugs that could inhibit Arp2/3 activity, CK666 and CK869, and dissected the mechanisms underlying these inhibitors (Hetrick et al., 2013), which upon binding between Arp2 and Arp3 subunits, prevent the change to an active conformation. We started by using CK869, to assess the effects Arp2/3 polimerization inhibition on cell morphology and the MPS. We were able to confirm that, at this concentration and acute treatment, CK869 was able to significantly reduce the percentage of MPS abundance in neurons at DIV5 and DIV14, thus suggesting that Arp2/3 participates in the formation and maintenance of the MPS.

To complement this, we moved to the genetic manipulation of cells to abolish the expression of Arp2/3. Our results showed that the CRISPR-Cas9 technique is effective and creates indels at the desired location. We also showed that neurons, including the mutant ARPC2 generated, do not present rings in DIV5 and DIV14, indicating that the Arp2/3 complex is very important for the formation and maintenance of the MPS. Although this observation is a novel finding in this field, Prokop's lab, using a distinct

system (Drosophila), has shown that reducing the expression of one of the Arp2/3 subunits, ARPC1, would trigger a reduction in the abundance of the MPS (Y. Qu et al., 2017). However, data related with Arp2/3 participation in the nucleation and elongation of the actin in rings within the MPS was missing.

We studied the endogenous expression of Arp2/3 using the p16 antibody, which refers to the ARPC5 subunit of the complex. Our results show that at early DIVs, there was a higher amount of ARPC5 than at later DIVs. The Arp2/3 complex comprises various subunits that present isoforms, such as Arp3, ARPC1, and ARPC5. However, the functional significance of these isoforms has not yet been thoroughly studied. Arp3 is present in all tissues, but there is an isoform called ARP3B mainly found in brain neurons, suggesting its potential role in neuronal development and maintenance. ARPC1 has two variants with 70% homology, and a mutation in ARPC1A has been linked to changes in cell migration and invasion in pancreatic cancer. ARPC1 also has a second isoform, ARPC1B, which is consistently expressed in many tissues, particularly in the brain, whereas the original ARPC1A is highly enriched in the spleen and thymus (Pizarro-Cerdá et al., 2017). In 2015, Abella et al., studied the different properties that the Arp2/3 complex can have based on the different isoforms that it can hold (Abella et al., 2016). Arp2/3 complexes that include ARPC1B and ARPC5L are more effective at stimulating actin assembly compared to complexes with ARPC1A and ARPC5 (Abella et al., 2016). Moreover, branched actin networks generated by complexes containing ARPC1B or ARPC5L exhibit a slower disassembly rate, implying that the Arp 2/3 complex is not a single structure as previously thought, but rather a very dynamic structure (Abella et al., 2016). Since ARPC5 appears to have an isoform, our results may indicate that at early DIVs ARPC5 is present, while at later DIVs ARPC5L is the one used to form the Arp2/3 complex. Further studies are required to dissect the functions of every isoform involved in the Arp2/3 complex and its presence in different DIVs.

Formins are another family of actin-binding proteins involved in the elongation of actin filaments. In 2009, a small molecule was characterized as an inhibitor of formins, SMIFH2 (Rizvi et al., 2009). Therefore, we started by using this drug to chemically modulate formins activity. Our findings show that at this concentration, SMIFH2 does not affect axon and dendrite length, and therefore, has no impact on cell morphology. The results obtained with STED microscopy showed that at early DIVs cells treated with SMIFH2 did not present an organized MPS. Conversely, at later DIVs, cells treated with SMIFH2 had actin rings and presented an organized MPS. This indicates that formins play a crucial role in the MPS' formation. However, when considering SMIFH2 results

some caution should be taken since recent studies have reported its effect on several other substrates beyond actin, such as microtubules, p53, and NMII which may contribute to SMIFH2-induced cytoskeletal remodelling (Nishimura et al., 2021). To further understand if and which formins participate in the MPS' formation, a genetic approach using shRNA was designed to reduce the expression of mDia1 and mDia2. These specific formins were chosen because both mDia1 and mDia2 are expressed in rat hippocampus (Monzo et al., 2016; Zhang et al., 2021). Both constructs appeared to be working, but further studies must confirm this. Our preliminary data using ShRNA targeting mDia1 and mDia2 supported the importance of formins in MPS formation.

The research developed during this thesis shows that both actin nucleators participate in the formation of the actin rings within the MPS whereas their maintenance is only affected by reduction of Arp2/3 levels. Currently, there are two hypotheses related to actin nucleation within the rings. Xiaowei Zhuang's laboratory inferred, based on the periodicity of adducin within this structure, that short filaments of actin form actin rings (Xu et al., 2013). In 2019, upon performing Platinum Replica EM studies coupled with super-resolution, Leterrier's laboratory suggested that actin rings were nucleated as two long intertwined filaments (Stéphane Vassilopoulos et al., 2019). Although these two hypotheses are still valid, one should consider that long structures are more challenged to adapt to changes in the diameter that accompany the axon and the neuron biochemistry (Costa et al., 2018). Overall, our data opens the perspective that during their early formation axonal actin rings are composed by both linear and branched actin filaments (dependent on Arp2/3 and formin-mediated nucleation) whereas their maintenance might be exclusively led by Arp2/3.

Conclusion and Future Perspectives

The MPS is a structure whose initial identification occurred a decade ago, with the development of super-resolution techniques. Since then, several questions have been answered. However, how this structure is formed, what molecules belong to this structure and the functions underlying the MPS are yet to be determined. It is our main aim to investigate how actin nucleates and elongates to form the ring within the MPS. Thus, this master thesis aimed at dissecting the role of the actin nucleators Arp2/3 and formins in the formation and maintenance of the MPS.

The results obtained suggest that the chemical inhibition of actin polymerization by CK869 and the depletion of Arp2/3 levels of expression are being successful strategies to developed our research, although more experiments aiming to increase the percentage of transfected neurons should be performed. STED nanoscopy studies show that both the nucleators are fundamental for MPS formation, since the percentage of MPS abundance is reduced either in chemical inhibitor or genetic experiments. Findings related to the endogenous expression of Arp2/3, as indicated by p16 staining (specific to the ARPC5 subunit), suggest higher expression levels at early DIVs compared to later stages. This thesis, thus, indicates the possibility of the existence of differential isoforms of Arp2/3 at different developmental stages of the neuron, being that ARPC5 is more expressed at initial DIVs whereas an alternative isoform, ARPC5L might be more expressed at later DIVs. To clarify this question, analyses of mRNA levels of all the subunits and their respective isoforms are being developed, as well as STED colocalization with actin.

Turning to formins, our preliminary results seem to indicate that this protein family plays a pivotal role in MPS formation. Further validation of the inhibition of expression of the specific formins analysed in this study are however needed, as well as additional STED analysis of the MPS of sh-downregulated neurons.

In summary, both Arp2/3 and formins appear to be prominently involved in MPS biology. While further investigations are needed to deepen our understanding, this information contributes significantly to unravelling the complexities surrounding the formation and maintenance of this vital cellular structure which highly contributes to the biology of neurons.

References

Abella, J. V. G., Galloni, C., Pernier, J., Barry, D. J., Kjær, S., Carlier, M.-F., & Way, M. (2016). Isoform diversity in the Arp2/3 complex determines actin filament dynamics. *Nature Cell Biology*, *18*(1), 76-86. https://doi.org/10.1038/ncb3286

Abouelezz, A., Stefen, H., Segerstrale, M., Micinski, D., Minkeviciene, R., Lahti, L., Hardeman, E. C., Gunning, P. W., Hoogenraad, C. C., Taira, T., Fath, T., & Hotulainen, P. (2020). Tropomyosin Tpm3.1 Is Required to Maintain the Structure and Function of the Axon Initial Segment. *iScience*, *23*(5), 101053. https://doi.org/10.1016/j.isci.2020.101053

Albrecht, D., Winterflood, C. M., Sadeghi, M., Tschager, T., Noe, F., & Ewers, H. (2016). Nanoscopic compartmentalization of membrane protein motion at the axon initial segment. *J Cell Biol*, *215*(1), 37-46. https://doi.org/10.1083/jcb.201603108

Amann, K. J., & Pollard, T. D. (2001). The Arp2/3 complex nucleates actin filament branches from the sides of pre-existing filaments. *Nat Cell Biol*, *3*(3), 306-310. https://doi.org/10.1038/35060104

Arimura, N., & Kaibuchi, K. (2007). Neuronal polarity: from extracellular signals to intracellular mechanisms. *Nature Reviews Neuroscience*, *8*(3), 194-205. https://doi.org/10.1038/nrn2056

Baas, P. W., & Lin, S. (2011). Hooks and comets: The story of microtubule polarity orientation in the neuron. *Dev Neurobiol*, *71*(6), 403-418. https://doi.org/10.1002/dneu.20818

Bartolini, F., Moseley, J. B., Schmoranzer, J., Cassimeris, L., Goode, B. L., & Gundersen, G. G. (2008). The formin mDia2 stabilizes microtubules independently of its actin nucleation activity. *J Cell Biol*, *181*(3), 523-536. https://doi.org/10.1083/jcb.200709029

Bazira, P. J. (2021). An overview of the nervous system. *Surgery (Oxford)*, *39*(8), 451-462. https://doi.org/https://doi.org/10.1016/j.mpsur.2021.06.012

Bennett, V., Davis, J., & Fowler, W. E. (1982). Brain spectrin, a membrane-associated protein related in structure and function to erythrocyte spectrin. *Nature*, *299*(5879), 126-131. https://doi.org/10.1038/299126a0

Berger, S. L., Leo-Macias, A., Yuen, S., Khatri, L., Pfennig, S., Zhang, Y., Agullo-Pascual, E., Caillol, G., Zhu, M. S., Rothenberg, E., Melendez-Vasquez, C. V., Delmar, M., Leterrier, C., & Salzer, J. L. (2018). Localized Myosin II Activity Regulates Assembly and Plasticity of the Axon Initial Segment. *Neuron*, *97*(3), 555-570 e556. https://doi.org/10.1016/j.neuron.2017.12.039

Bradke, F., & Dotti, C. G. (2000). Establishment of neuronal polarity: lessons from cultured hippocampal neurons. *Current Opinion in Neurobiology*, *10*(5), 574-581. https://doi.org/https://doi.org/10.1016/S0959-4388(00)00124-0

Brodal, P. (2004). *The central nervous system: structure and function*. oxford university Press.

Chalkia, D., Nikolaidis, N., Makalowski, W., Klein, J., & Nei, M. (2008). Origins and evolution of the formin multigene family that is involved in the formation of actin filaments. *Mol Biol Evol*, *25*(12), 2717-2733. https://doi.org/10.1093/molbev/msn215

Chan, F. Y., Silva, A. M., Saramago, J., Pereira-Sousa, J., Brighton, H. E., Pereira, M., Oegema, K., Gassmann, R., & Carvalho, A. X. (2019). The ARP2/3 complex prevents excessive formin activity during cytokinesis. *Mol Biol Cell*, *30*(1), 96-107. https://doi.org/10.1091/mbc.E18-07-0471

Chesarone, M. A., DuPage, A. G., & Goode, B. L. (2010). Unleashing formins to remodel the actin and microtubule cytoskeletons. *Nature Reviews Molecular Cell Biology*, *11*(1), 62-74. https://doi.org/10.1038/nrm2816

Conde, C., & Cáceres, A. (2009). Microtubule assembly, organization and dynamics in axons and dendrites. *Nat Rev Neurosci*, *10*(5), 319-332. https://doi.org/10.1038/nrn2631

Cooper, G. M., & Adams, K. (2023). *The cell: a molecular approach*. Oxford University Press.

Cooper, J. A., Wear, M. A., & Weaver, A. M. (2001). Arp2/3 Complex: Advances on the Inner Workings of a Molecular Machine. *Cell*, *107*(6), 703-705. https://doi.org/10.1016/S0092-8674(01)00605-5

Costa, A. R., Pinto-Costa, R., Sousa, S. C., & Sousa, M. M. (2018). The Regulation of Axon Diameter: From Axonal Circumferential Contractility to Activity-Dependent Axon Swelling. *Front Mol Neurosci*, *11*, 319. https://doi.org/10.3389/fnmol.2018.00319

Costa, A. R., & Sousa, M. M. (2021). The role of the membrane-associated periodic skeleton in axons. *Cell Mol Life Sci*, *78*(13), 5371-5379. https://doi.org/10.1007/s00018-021-03867-x

Costa, A. R., Sousa, S. C., Pinto-Costa, R., Mateus, J. C., Lopes, C. D., Costa, A. C., Rosa, D., Machado, D., Pajuelo, L., Wang, X., Zhou, F. Q., Pereira, A. J., Sampaio, P., Rubinstein, B. Y., Mendes Pinto, I., Lampe, M., Aguiar, P., & Sousa, M. M. (2020). The membrane periodic skeleton is an actomyosin network that

regulates axonal diameter and conduction. *Elife*, *9*. https://doi.org/10.7554/eLife.55471

Courtemanche, N. (2018). Mechanisms of formin-mediated actin assembly and dynamics. *Biophys Rev*, *10*(6), 1553-1569. https://doi.org/10.1007/s12551-018-0468-6

Craig, A. M., & Banker, G. (1994). Neuronal polarity. *Annu Rev Neurosci*, *17*, 267-310. https://doi.org/10.1146/annurev.ne.17.030194.001411

D'Este, E., Kamin, D., Balzarotti, F., & Hell, S. W. (2017). Ultrastructural anatomy of nodes of Ranvier in the peripheral nervous system as revealed by STED microscopy. *Proc Natl Acad Sci U S A*, *114*(2), E191-E199. https://doi.org/10.1073/pnas.1619553114

D'Este, E., Kamin, D., Gottfert, F., El-Hady, A., & Hell, S. W. (2015). STED nanoscopy reveals the ubiquity of subcortical cytoskeleton periodicity in living neurons. *Cell Rep*, *10*(8), 1246-1251. https://doi.org/10.1016/j.celrep.2015.02.007

D'Este, E., Kamin, D., Velte, C., Gottfert, F., Simons, M., & Hell, S. W. (2016). Subcortical cytoskeleton periodicity throughout the nervous system. *Sci Rep*, *6*, 22741. https://doi.org/10.1038/srep22741

Dayel, M. J., & Mullins, R. D. (2004). Activation of Arp2/3 complex: addition of the first subunit of the new filament by a WASP protein triggers rapid ATP hydrolysis on Arp2. *PLoS Biol*, *2*(4), E91. https://doi.org/10.1371/journal.pbio.0020091

Debanne, D., Campanac, E., Bialowas, A., Carlier, E., & Alcaraz, G. (2011). Axon Physiology. *Physiological Reviews*, *91*(2), 555-602. https://doi.org/10.1152/physrev.00048.2009

Dharani, K. (2015). Chapter 2 - Physiology of the Neuron. In K. Dharani (Ed.), *The Biology of Thought* (pp. 31-52). Academic Press. https://doi.org/https://doi.org/10.1016/B978-0-12-800900-0.00002-6

Dominguez, R. (2004). Actin-binding proteins – a unifying hypothesis. *Trends in Biochemical Sciences*, *29*(11), 572-578. https://doi.org/https://doi.org/10.1016/j.tibs.2004.09.004

Dominguez, R., & Holmes, K. C. (2011). Actin structure and function. *Annu Rev Biophys*, *40*, 169-186. https://doi.org/10.1146/annurev-biophys-042910-155359

Dubey, S., Bhembre, N., Bodas, S., Veer, S., Ghose, A., Callan-Jones, A., & Pullarkat, P. (2020). The axonal actin-spectrin lattice acts as a tension buffering shock absorber. *Elife*, *9*. https://doi.org/10.7554/eLife.51772

Duch, C., & Ryglewski, S. (2016). Structure and function of neuronal dendrites. *e-Neuroforum*, *7*(4), 71-81. https://doi.org/10.1007/s13295-016-0032-4

Egile, C., Rouiller, I., Xu, X. P., Volkmann, N., Li, R., & Hanein, D. (2005). Mechanism of filament nucleation and branch stability revealed by the structure of the Arp2/3 complex at actin branch junctions. *PLoS Biol*, *3*(11), e383. https://doi.org/10.1371/journal.pbio.0030383

Evangelista, M., Zigmond, S., & Boone, C. (2003). Formins: signaling effectors for assembly and polarization of actin filaments. *Journal of Cell Science*, *116*(13), 2603-2611. https://doi.org/10.1242/jcs.00611

Gaillard, J., Ramabhadran, V., Neumanne, E., Gurel, P., Blanchoin, L., Vantard, M., & Higgs, H. N. (2011). Differential interactions of the formins INF2, mDia1, and mDia2 with microtubules. *Molecular Biology of the Cell*, *22*(23), 4575-4587.

Galiano, M. R., Jha, S., Ho, T. S., Zhang, C., Ogawa, Y., Chang, K. J., Stankewich, M. C., Mohler, P. J., & Rasband, M. N. (2012). A distal axonal cytoskeleton forms an intra-axonal boundary that controls axon initial segment assembly. *Cell*, *149*(5), 1125-1139. https://doi.org/10.1016/j.cell.2012.03.039

Gallardo, G., Barowski, J., Ravits, J., Siddique, T., Lingrel, J. B., Robertson, J., Steen, H., & Bonni, A. (2014). An alpha2-Na/K ATPase/alpha-adducin complex in astrocytes triggers non-cell autonomous neurodegeneration. *Nat Neurosci*, *17*(12), 1710-1719. https://doi.org/10.1038/nn.3853

Ghoshdastider, U., Popp, D., Burtnick, L. D., & Robinson, R. C. (2013). The expanding superfamily of gelsolin homology domain proteins. *Cytoskeleton*, *70*(11), 775-795. https://doi.org/https://doi.org/10.1002/cm.21149

Goh, W. I., & Ahmed, S. (2012). mDia1-3 in mammalian filopodia. *Communicative & Integrative Biology*, *5*(4), 340-344. https://doi.org/10.4161/cib.20214

Goley, E. D., & Welch, M. D. (2006). The ARP2/3 complex: an actin nucleator comes of age. *Nature Reviews Molecular Cell Biology*, *7*(10), 713-726. https://doi.org/10.1038/nrm2026

Goode, B. L., & Eck, M. J. (2007). Mechanism and Function of Formins in the Control of Actin Assembly. *Annual Review of Biochemistry*, *76*(1), 593-627. https://doi.org/10.1146/annurev.biochem.75.103004.142647

Gregorio, C. C., Weber, A., Bondad, M., Pennise, C. R., & Fowler, V. M. (1995). Requirement of pointed-end capping by tropomodulin to maintain actin filament length in embryonic chick cardiac myocytes. *Nature*, *377*(6544), 83-86. https://doi.org/10.1038/377083a0

Hamdan, H., Lim, B. C., Torii, T., Joshi, A., Konning, M., Smith, C., Palmer, D. J., Ng, P., Leterrier, C., Oses-Prieto, J. A., Burlingame, A. L., & Rasband, M. N. (2020). Mapping axon initial segment structure and function by multiplexed proximity

biotinylation. *Nat Commun*, *11*(1), 100. https://doi.org/10.1038/s41467-019-13658-5

Hammond, C. (2015). Chapter 1 - Neurons. In C. Hammond (Ed.), *Cellular and Molecular Neurophysiology (Fourth Edition)* (pp. 3-23). Academic Press. https://doi.org/https://doi.org/10.1016/B978-0-12-397032-9.00001-7

Han, B., Zhou, R., Xia, C., & Zhuang, X. (2017). Structural organization of the actin-spectrin-based membrane skeleton in dendrites and soma of neurons. *Proc Natl Acad Sci U S A*, *114*(32), E6678-E6685. https://doi.org/10.1073/pnas.1705043114

Hannappel, E. (2007). beta-Thymosins. *Annals of the New York Academy of Sciences*, *1112*, 21-37. https://doi.org/10.1196/annals.1415.018

Hauser, M., Yan, R., Li, W., Repina, N. A., Schaffer, D. V., & Xu, K. (2018). The Spectrin-Actin-Based Periodic Cytoskeleton as a Conserved Nanoscale Scaffold and Ruler of the Neural Stem Cell Lineage. *Cell Rep*, *24*(6), 1512-1522. https://doi.org/10.1016/j.celrep.2018.07.005

He, J., Zhou, R., Wu, Z., Carrasco, M. A., Kurshan, P. T., Farley, J. E., Simon, D. J., Wang, G., Han, B., Hao, J., Heller, E., Freeman, M. R., Shen, K., Maniatis, T., Tessier-Lavigne, M., & Zhuang, X. (2016). Prevalent presence of periodic actin-spectrin-based membrane skeleton in a broad range of neuronal cell types and animal species. *Proc Natl Acad Sci U S A*, *113*(21), 6029-6034. https://doi.org/10.1073/pnas.1605707113

Hetrick, B., Han, M. S., Helgeson, L. A., & Nolen, B. J. (2013). Small molecules CK-666 and CK-869 inhibit actin-related protein 2/3 complex by blocking an activating conformational change. *Chem Biol*, *20*(5), 701-712. https://doi.org/10.1016/j.chembiol.2013.03.019

Higgs, H. N. (2005). Formin proteins: a domain-based approach. *Trends Biochem Sci*, *30*(6), 342-353. https://doi.org/10.1016/j.tibs.2005.04.014

Huang, C. Y.-M., & Rasband, M. N. (2018). Axon initial segments: structure, function, and disease. *Annals of the New York Academy of Sciences*, *1420*(1), 46-61. https://doi.org/https://doi.org/10.1111/nyas.13718

Huang, C. Y., Zhang, C., Ho, T. S., Oses-Prieto, J., Burlingame, A. L., Lalonde, J., Noebels, J. L., Leterrier, C., & Rasband, M. N. (2017). alphaII Spectrin Forms a Periodic Cytoskeleton at the Axon Initial Segment and Is Required for Nervous System Function. *J Neurosci*, *37*(47), 11311-11322. https://doi.org/10.1523/JNEUROSCI.2112-17.2017

Jégou, A., Carlier, M. F., & Romet-Lemonne, G. (2013). Formin mDia1 senses and generates mechanical forces on actin filaments. *Nat Commun*, *4*, 1883. https://doi.org/10.1038/ncomms2888

Jones, S. L., & Svitkina, T. M. (2016). Axon Initial Segment Cytoskeleton: Architecture, Development, and Role in Neuron Polarity. *Neural Plasticity*, *2016*, 6808293. https://doi.org/10.1155/2016/6808293

Kevenaar, J. T., & Hoogenraad, C. C. (2015). The axonal cytoskeleton: from organization to function [Review]. *Frontiers in Molecular Neuroscience*, *8*. https://www.frontiersin.org/articles/10.3389/fnmol.2015.00044

Koch, C., & Laurent, G. (1999). Complexity and the Nervous System. *Science*, *284*(5411), 96-98. https://doi.org/doi:10.1126/science.284.5411.96

Kovar, D. R. (2006). Molecular details of formin-mediated actin assembly. *Curr Opin Cell Biol*, *18*(1), 11-17. https://doi.org/10.1016/j.ceb.2005.12.011

Kruer, M. C., Jepperson, T., Dutta, S., Steiner, R. D., Cottenie, E., Sanford, L., Merkens, M., Russman, B. S., Blasco, P. A., Fan, G., Pollock, J., Green, S., Woltjer, R. L., Mooney, C., Kretzschmar, D., Paisan-Ruiz, C., & Houlden, H. (2013). Mutations in gamma adducin are associated with inherited cerebral palsy. *Ann Neurol*, *74*(6), 805-814. https://doi.org/10.1002/ana.23971

Lappalainen, P. (2016). Actin-binding proteins: the long road to understanding the dynamic landscape of cellular actin networks. *Molecular Biology of the Cell*, *27*(16), 2519-2522. https://doi.org/10.1091/mbc.e15-10-0728

Leite, S. C., Sampaio, P., Sousa, V. F., Nogueira-Rodrigues, J., Pinto-Costa, R., Peters, L. L., Brites, P., & Sousa, M. M. (2016a). The Actin-Binding Protein alpha-Adducin Is Required for Maintaining Axon Diameter. *Cell Rep*, *15*(3), 490-498. https://doi.org/10.1016/j.celrep.2016.03.047

Leite, S. C., Sampaio, P., Sousa, V. F., Nogueira-Rodrigues, J., Pinto-Costa, R., Peters, L. L., Brites, P., & Sousa, M. M. (2016b). The Actin-Binding Protein α-Adducin Is Required for Maintaining Axon Diameter. *Cell Rep*, *15*(3), 490-498. https://doi.org/10.1016/j.celrep.2016.03.047

Leite, S. C., & Sousa, M. M. (2016). The neuronal and actin commitment: Why do neurons need rings? *Cytoskeleton (Hoboken)*, *73*(9), 424-434. https://doi.org/10.1002/cm.21273

Leterrier, C. (2016). Chapter Six - The Axon Initial Segment, 50Years Later: A Nexus for Neuronal Organization and Function. In V. Bennett (Ed.), *Current Topics in Membranes* (Vol. 77, pp. 185-233). Academic Press. https://doi.org/https://doi.org/10.1016/bs.ctm.2015.10.005

Leterrier, C. (2018). The Axon Initial Segment: An Updated Viewpoint. *The Journal of Neuroscience*, *38*(9), 2135-2145. https://doi.org/10.1523/jneurosci.1922-17.2018

Leterrier, C., Dubey, P., & Roy, S. (2017). The nano-architecture of the axonal cytoskeleton. *Nat Rev Neurosci*, *18*(12), 713-726. https://doi.org/10.1038/nrn.2017.129

Libersat, F. (2005). Maturation of dendritic architecture: Lessons from insect identified neurons. *Journal of Neurobiology*, *64*(1), 11-23. https://doi.org/https://doi.org/10.1002/neu.20142

Lovinger, D. M. (2008). Communication networks in the brain: neurons, receptors, neurotransmitters, and alcohol. *Alcohol Res Health*, *31*(3), 196-214.

Ludwig, P., & Varacallo, M. (2018). Neuroanatomy, Central Nervous System (CNS).

Lukinavicius, G., Reymond, L., D'Este, E., Masharina, A., Gottfert, F., Ta, H., Guther, A., Fournier, M., Rizzo, S., Waldmann, H., Blaukopf, C., Sommer, C., Gerlich, D. W., Arndt, H. D., Hell, S. W., & Johnsson, K. (2014). Fluorogenic probes for live-cell imaging of the cytoskeleton. *Nat Methods*, *11*(7), 731-733. https://doi.org/10.1038/nmeth.2972

Maiti, S., Michelot, A., Gould, C., Blanchoin, L., Sokolova, O., & Goode, B. L. (2012). Structure and activity of full-length formin mDia1. *Cytoskeleton (Hoboken)*, *69*(6), 393-405. https://doi.org/10.1002/cm.21033

Mei, Y., Han, X., Liu, Y., Yang, J., Sumagin, R., & Ji, P. (2020). Diaphanous-related formin mDia2 regulates beta2 integrins to control hematopoietic stem and progenitor cell engraftment. *Nature Communications*, *11*(1), 3172. https://doi.org/10.1038/s41467-020-16911-4

Menon, S., & Gupton, S. L. (2016). Building Blocks of Functioning Brain: Cytoskeletal Dynamics in Neuronal Development. In *International Review of Cell and Molecular Biology* (pp. 183-245). Elsevier. https://doi.org/10.1016/bs.ircmb.2015.10.002

Merino, F., Pospich, S., & Raunser, S. (2020). Towards a structural understanding of the remodeling of the actin cytoskeleton. *Seminars in Cell & Developmental Biology*, *102*, 51-64. https://doi.org/https://doi.org/10.1016/j.semcdb.2019.11.018

Mihailoff, G. A., & Haines, D. E. (2018). Chapter 2 - The Cell Biology of Neurons and Glia. In D. E. Haines & G. A. Mihailoff (Eds.), *Fundamental Neuroscience for Basic and Clinical Applications (Fifth Edition)* (pp. 15-33.e11). Elsevier. https://doi.org/https://doi.org/10.1016/B978-0-323-39632-5.00002-5

Mizuno, H., Higashida, C., Yuan, Y., Ishizaki, T., Narumiya, S., & Watanabe, N. (2011). Rotational movement of the formin mDia1 along the double helical strand of an

actin filament. *Science*, *331*(6013), 80-83. https://doi.org/10.1126/science.1197692

Monzo, P., Chong, Y. K., Guetta-Terrier, C., Krishnasamy, A., Sathe, S. R., Yim, E. K. F., Ng, W. H., Ang, B. T., Tang, C., Ladoux, B., Gauthier, N. C., & Sheetz, M. P. (2016). Mechanical confinement triggers glioma linear migration dependent on formin FHOD3. *Molecular Biology of the Cell*, *27*(8), 1246-1261. https://doi.org/10.1091/mbc.E15-08-0565

Moseley, J. B., Maiti, S., & Goode, B. L. (2006). Formin proteins: purification and measurement of effects on actin assembly. *Methods Enzymol*, *406*, 215-234. https://doi.org/10.1016/s0076-6879(06)06016-2

Muzio, M. R., & Cascella, M. (2022). *Histology, Axon*. StatPearls Publishing, Treasure Island (FL). http://europepmc.org/abstract/MED/32119275

http://europepmc.org/books/NBK554388

https://www.ncbi.nlm.nih.gov/books/NBK554388

Neukirchen, D., & Bradke, F. (2011). Neuronal polarization and the cytoskeleton. *Semin Cell Dev Biol*, *22*(8), 825-833. https://doi.org/10.1016/j.semcdb.2011.08.007

Nezami, A. G., Poy, F., & Eck, M. J. (2006). Structure of the autoinhibitory switch in formin mDia1. *Structure*, *14*(2), 257-263. https://doi.org/10.1016/j.str.2005.12.003

Nishimura, Y., Shi, S., Zhang, F., Liu, R., Takagi, Y., Bershadsky, A. D., Viasnoff, V., & Sellers, J. R. (2021). The formin inhibitor SMIFH2 inhibits members of the myosin superfamily. *J Cell Sci*, *134*(8). https://doi.org/10.1242/jcs.253708

Padrick, S. B., Doolittle, L. K., Brautigam, C. A., King, D. S., & Rosen, M. K. (2011). Arp2/3 complex is bound and activated by two WASP proteins. *Proc Natl Acad Sci U S A*, *108*(33), E472-479. https://doi.org/10.1073/pnas.1100236108

Paul, A. S., & Pollard, T. D. (2009). Review of the mechanism of processive actin filament elongation by formins. *Cell Motil Cytoskeleton*, *66*(8), 606-617. https://doi.org/10.1002/cm.20379

Pittenger, M. F., Kazzaz, J. A., & Helfman, D. M. (1994). Functional properties of non-muscle tropomyosin isoforms. *Current Opinion in Cell Biology*, *6*(1), 96-104. https://doi.org/https://doi.org/10.1016/0955-0674(94)90122-8

Pizarro-Cerdá, J., Chorev, D. S., Geiger, B., & Cossart, P. (2017). The Diverse Family of Arp2/3 Complexes. *Trends Cell Biol*, *27*(2), 93-100. https://doi.org/10.1016/j.tcb.2016.08.001

Pollard, T. D. (2011). Formin Tip Tracking. *Science*, *331*(6013), 39-41. https://doi.org/doi:10.1126/science.1200773

Pollard, T. D. (2016). Actin and Actin-Binding Proteins. *Cold Spring Harb Perspect Biol*, *8*(8). https://doi.org/10.1101/cshperspect.a018226

Prokop, A. (2020). Cytoskeletal organization of axons in vertebrates and invertebrates. *Journal of Cell Biology*, *219*(7). https://doi.org/10.1083/jcb.201912081

Purves, D., Augustine, G. J., Fitzpatrick, D., Hall, W. C., LaMantia, A.-S., McNamara, J. O., & Williams, S. M. (Eds.). (2004). *Neuroscience, 3rd ed*. Sinauer Associates.

Purves, D., & Lichtman, J. W. (1985). Geometrical Differences Among Homologous Neurons in Mammals. *Science*, *228*(4697), 298-302. https://doi.org/doi:10.1126/science.3983631

Qu, X., Yuan, F. N., Corona, C., Pasini, S., Pero, M. E., Gundersen, G. G., Shelanski, M. L., & Bartolini, F. (2017). Stabilization of dynamic microtubules by mDia1 drives Tau-dependent Aβ(1-42) synaptotoxicity. *J Cell Biol*, *216*(10), 3161-3178. https://doi.org/10.1083/jcb.201701045

Qu, Y., Hahn, I., Webb, S. E., Pearce, S. P., & Prokop, A. (2017). Periodic actin structures in neuronal axons are required to maintain microtubules. *Mol Biol Cell*, *28*(2), 296-308. https://doi.org/10.1091/mbc.E16-10-0727

Rao, J. N., Madasu, Y., & Dominguez, R. (2014). Mechanism of actin filament pointed-end capping by tropomodulin. *Science*, *345*(6195), 463-467. https://doi.org/10.1126/science.1256159

Remedios, C. G. D., Chhabra, D., Kekic, M., Dedova, I. V., Tsubakihara, M., Berry, D. A., & Nosworthy, N. J. (2003). Actin Binding Proteins: Regulation of Cytoskeletal Microfilaments. *Physiological Reviews*, *83*(2), 433-473. https://doi.org/10.1152/physrev.00026.2002

Rief, M., Pascual, J., Saraste, M., & Gaub, H. E. (1999). Single molecule force spectroscopy of spectrin repeats: low unfolding forces in helix bundles. *J Mol Biol*, *286*(2), 553-561. https://doi.org/10.1006/jmbi.1998.2466

Rizvi, S. A., Neidt, E. M., Cui, J., Feiger, Z., Skau, C. T., Gardel, M. L., Kozmin, S. A., & Kovar, D. R. (2009). Identification and characterization of a small molecule inhibitor of formin-mediated actin assembly. *Chem Biol*, *16*(11), 1158-1168. https://doi.org/10.1016/j.chembiol.2009.10.006

Rouiller, I., Xu, X. P., Amann, K. J., Egile, C., Nickell, S., Nicastro, D., Li, R., Pollard, T. D., Volkmann, N., & Hanein, D. (2008). The structural basis of actin filament branching by the Arp2/3 complex. *J Cell Biol*, *180*(5), 887-895. https://doi.org/10.1083/jcb.200709092

Roy, S. (2016). Waves, rings, and trails: The scenic landscape of axonal actin. *J Cell Biol*, *212*(2), 131-134. https://doi.org/10.1083/jcb.201511016

Schroer, T. A., Fyrberg, E., Cooper, J. A., Waterston, R. H., Helfman, D., Pollard, T. D., & Meyer, D. I. (1994). Actin-related protein nomenclature and classification. *J Cell Biol*, *127*(6 Pt 2), 1777-1778. https://doi.org/10.1083/jcb.127.6.1777

Shotton, D. M., Burke, B. E., & Branton, D. (1979). The molecular structure of human erythrocyte spectrin. *Journal of Molecular Biology*, *131*(2), 303-329. https://doi.org/10.1016/0022-2836(79)90078-0

Smith, B. A., Daugherty-Clarke, K., Goode, B. L., & Gelles, J. (2013). Pathway of actin filament branch formation by Arp2/3 complex revealed by single-molecule imaging. *Proc Natl Acad Sci U S A*, *110*(4), 1285-1290. https://doi.org/10.1073/pnas.1211164110

Squire, L. (2013). *Fundamental Neuroscience*. Elsevier Science. https://books.google.pt/books?id=AEmEn-_hD9IC

Stankewich, M. C., Gwynn, B., Ardito, T., Ji, L., Kim, J., Robledo, R. F., Lux, S. E., Peters, L. L., & Morrow, J. S. (2010). Targeted deletion of betaIII spectrin impairs synaptogenesis and generates ataxic and seizure phenotypes. *Proc Natl Acad Sci U S A*, *107*(13), 6022-6027. https://doi.org/10.1073/pnas.1001522107

Stiess, M., & Bradke, F. (2011). Neuronal polarization: the cytoskeleton leads the way. *Dev Neurobiol*, *71*(6), 430-444. https://doi.org/10.1002/dneu.20849

Südhof, T. C. (2012). The presynaptic active zone. *Neuron*, *75*(1), 11-25. https://doi.org/10.1016/j.neuron.2012.06.012

Sun, H. Q., Yamamoto, M., Mejillano, M., & Yin, H. L. (1999). Gelsolin, a Multifunctional Actin Regulatory Protein*. *Journal of Biological Chemistry*, *274*(47), 33179-33182. https://doi.org/https://doi.org/10.1074/jbc.274.47.33179

Sutherland-Smith, A. J. (2011). Filamin structure, function and mechanics: are altered filamin-mediated force responses associated with human disease? *Biophys Rev*, *3*(1), 15-23. https://doi.org/10.1007/s12551-011-0042-y

Tahirovic, S., & Bradke, F. (2009). Neuronal polarity. *Cold Spring Harb Perspect Biol*, *1*(3), a001644. https://doi.org/10.1101/cshperspect.a001644

Takano, T., Xu, C., Funahashi, Y., Namba, T., & Kaibuchi, K. (2015). Neuronal polarization. *Development*, *142*(12), 2088-2093. https://doi.org/10.1242/dev.114454

Tavosanis, G. (2012). Dendritic structural plasticity. *Developmental Neurobiology*, *72*(1), 73-86. https://doi.org/https://doi.org/10.1002/dneu.20951

Terni, B., & Llobet, A. (2021). Axon terminals control endolysosome diffusion to support synaptic remodelling. *Life Sci Alliance*, *4*(8). https://doi.org/10.26508/lsa.202101105

Tominaga, T., Sahai, E., Chardin, P., McCormick, F., Courtneidge, S. A., & Alberts, A. S. (2000). Diaphanous-related formins bridge Rho GTPase and Src tyrosine kinase signaling. *Mol Cell*, *5*(1), 13-25. https://doi.org/10.1016/s1097-2765(00)80399-8

Unsain, N., Bordenave, M. D., Martinez, G. F., Jalil, S., von Bilderling, C., Barabas, F. M., Masullo, L. A., Johnstone, A. D., Barker, P. A., Bisbal, M., Stefani, F. D., & Caceres, A. O. (2018). Remodeling of the Actin/Spectrin Membrane-associated Periodic Skeleton, Growth Cone Collapse and F-Actin Decrease during Axonal Degeneration. *Sci Rep*, *8*(1), 3007. https://doi.org/10.1038/s41598-018-21232-0

Unsain, N., Stefani, F. D., & Cáceres, A. (2018). The Actin/Spectrin Membrane-Associated Periodic Skeleton in Neurons [Mini Review]. *Frontiers in Synaptic Neuroscience*, *10*. https://doi.org/10.3389/fnsyn.2018.00010

Uribe, R., & Jay, D. (2009). A review of actin binding proteins: new perspectives. *Molecular Biology Reports*, *36*(1), 121-125. https://doi.org/10.1007/s11033-007-9159-2

Vassilopoulos, S., Gibaud, S., Jimenez, A., Caillol, G., & Leterrier, C. (2019). Ultrastructure of the axonal periodic scaffold reveals a braid-like organization of actin rings. *Nat Commun*, *10*(1), 5803. https://doi.org/10.1038/s41467-019-13835-6

Vassilopoulos, S., Gibaud, S., Jimenez, A., Caillol, G., & Leterrier, C. (2019). Ultrastructure of the axonal periodic scaffold reveals a braid-like organization of actin rings. *Nature Communications*, *10*(1), 5803. https://doi.org/10.1038/s41467-019-13835-6

Wang, G., Simon, D. J., Wu, Z., Belsky, D. M., Heller, E., O'Rourke, M. K., Hertz, N. T., Molina, H., Zhong, G., Tessier-Lavigne, M., & Zhuang, X. (2019). Structural plasticity of actin-spectrin membrane skeleton and functional role of actin and spectrin in axon degeneration. *Elife*, *8*. https://doi.org/10.7554/eLife.38730

Wang, T., Li, W., Martin, S., Papadopulos, A., Joensuu, M., Liu, C., Jiang, A., Shamsollahi, G., Amor, R., Lanoue, V., Padmanabhan, P., & Meunier, F. A. (2020). Radial contractility of actomyosin rings facilitates axonal trafficking and structural stability. *J Cell Biol*, *219*(5). https://doi.org/10.1083/jcb.201902001

Wioland, H., Guichard, B., Senju, Y., Myram, S., Lappalainen, P., Jégou, A., & Romet-Lemonne, G. (2017). ADF/Cofilin Accelerates Actin Dynamics by Severing

Filaments and Promoting Their Depolymerization at Both Ends. *Curr Biol*, *27*(13), 1956-1967.e1957. https://doi.org/10.1016/j.cub.2017.05.048

Witke, W., Podtelejnikov, A. V., Di Nardo, A., Sutherland, J. D., Gurniak, C. B., Dotti, C., & Mann, M. (1998). In mouse brain profilin I and profilin II associate with regulators of the endocytic pathway and actin assembly. *Embo j*, *17*(4), 967-976. https://doi.org/10.1093/emboj/17.4.967

Witte, H., & Bradke, F. (2008). The role of the cytoskeleton during neuronal polarization. *Current Opinion in Neurobiology*, *18*(5), 479-487. https://doi.org/https://doi.org/10.1016/j.conb.2008.09.019

Xu, K., Zhong, G., & Zhuang, X. (2013). Actin, spectrin, and associated proteins form a periodic cytoskeletal structure in axons. *Science*, *339*(6118), 452-456. https://doi.org/10.1126/science.1232251

Yamada, R., & Kuba, H. (2016). Structural and Functional Plasticity at the Axon Initial Segment [Mini Review]. *Frontiers in Cellular Neuroscience*, *10*. https://doi.org/10.3389/fncel.2016.00250

Yamashita, A., Maeda, K., & Maéda, Y. (2003). Crystal structure of CapZ: structural basis for actin filament barbed end capping. *Embo j*, *22*(7), 1529-1538. https://doi.org/10.1093/emboj/cdg167

Yang, C., Czech, L., Gerboth, S., Kojima, S., Scita, G., & Svitkina, T. (2007). Novel roles of formin mDia2 in lamellipodia and filopodia formation in motile cells. *PLoS Biol*, *5*(11), e317. https://doi.org/10.1371/journal.pbio.0050317

Yu, M., Yuan, X., Lu, C., Le, S., Kawamura, R., Efremov, A. K., Zhao, Z., Kozlov, M. M., Sheetz, M., Bershadsky, A., & Yan, J. (2017). mDia1 senses both force and torque during F-actin filament polymerization. *Nat Commun*, *8*(1), 1650. https://doi.org/10.1038/s41467-017-01745-4

Yuan, A., Rao, M. V., Veeranna, & Nixon, R. A. (2012). Neurofilaments at a glance. *J Cell Sci*, *125*(Pt 14), 3257-3263. https://doi.org/10.1242/jcs.104729

Yuan, A., Sasaki, T., Rao, M. V., Kumar, A., Kanumuri, V., Dunlop, D. S., Liem, R. K., & Nixon, R. A. (2009). Neurofilaments form a highly stable stationary cytoskeleton after reaching a critical level in axons. *J Neurosci*, *29*(36), 11316-11329. https://doi.org/10.1523/jneurosci.1942-09.2009

Zhang, W., Ciorraga, M., Mendez, P., Retana, D., Boumedine-Guignon, N., Achón, B., Russier, M., Debanne, D., & Garrido, J. J. (2021). Formin Activity and mDia1 Contribute to Maintain Axon Initial Segment Composition and Structure. *Mol Neurobiol*, *58*(12), 6153-6169. https://doi.org/10.1007/s12035-021-02531-6

Zhang, Y., Tzingounis, A. V., & Lykotrafitis, G. (2019). Modeling of the axon plasma membrane structure and its effects on protein diffusion. *PLoS Comput Biol*, *15*(5), e1007003. https://doi.org/10.1371/journal.pcbi.1007003

Zhong, G., He, J., Zhou, R., Lorenzo, D., Babcock, H. P., Bennett, V., & Zhuang, X. (2014). Developmental mechanism of the periodic membrane skeleton in axons. *Elife*, *3*. https://doi.org/10.7554/eLife.04581

Zhou, R., Han, B., Nowak, R., Lu, Y., Heller, E., Xia, C., Chishti, A. H., Fowler, V. M., & Zhuang, X. (2020). Proteomic and functional analyses of the periodic membrane skeleton in neurons. https://doi.org/10.1101/2020.12.23.424206

Zhou, R., Han, B., Xia, C., & Zhuang, X. (2019). Membrane-associated periodic skeleton is a signaling platform for RTK transactivation in neurons. *Science*, *365*(6456), 929-934. https://doi.org/10.1126/science.aaw5937